NASA TECHNICAL NOTE

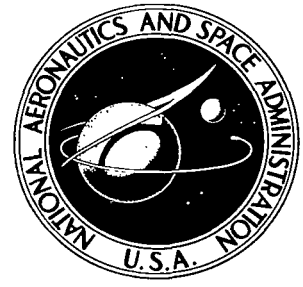

NASA TN D-8297

LASER DOPPLER VELOCIMETER SYSTEM FOR TURBINE STATOR CASCADE STUDIES AND ANALYSIS OF STATISTICAL BIASING ERRORS

Richard G. Seasholtz

Lewis Research Center
Cleveland, Ohio 44135

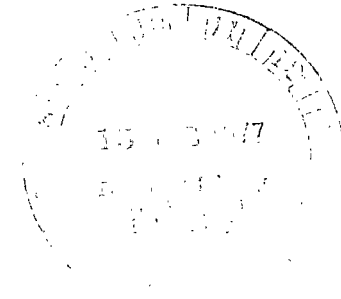

NATIONAL AERONAUTICS AND SPACE ADMINISTRATION • WASHINGTON, D. C. • FEBRUARY 1977

1. Report No.	2. Government Accession No.	3. Recipient's Catalog No.
NASA TN D-8297		

4. Title and Subtitle
LASER DOPPLER VELOCIMETER SYSTEM FOR TURBINE STATOR CASCADE STUDIES AND ANALYSIS OF STATISTICAL BIASING ERRORS

5. Report Date
February 1977

6. Performing Organization Code

7. Author(s)
Richard G. Seasholtz

8. Performing Organization Report No.
E-8799

9. Performing Organization Name and Address
Lewis Research Center
National Aeronautics and Space Administration
Cleveland, Ohio 44135

10. Work Unit No.
505-04

11. Contract or Grant No.

12. Sponsoring Agency Name and Address
National Aeronautics and Space Administration
Washington, D.C. 20546

13. Type of Report and Period Covered
Technical Note

14. Sponsoring Agency Code

15. Supplementary Notes

16. Abstract

A laser Doppler velocimeter (LDV) built for use in the Lewis Research Center's turbine stator cascade facilities is described. The signal processing and self-contained data processing are based on a computing counter. A procedure is given for mode matching the laser to the probe volume. An analysis is presented of biasing errors that were observed in turbulent flow when the mean flow was not normal to the fringes.

17. Key Words (Suggested by Author(s))	18. Distribution Statement
Laser Doppler velocimeters; Turbulent flow; Axial flow turbines; Flow measurement; Optical measuring instruments; Velocity measurement; Turbulence meters; Turbine instruments	Unclassified - unlimited STAR Category 35

19. Security Classif. (of this report)	20. Security Classif. (of this page)	21. No. of Pages	22. Price*
Unclassified	Unclassified	47	$4.00

* For sale by the National Technical Information Service, Springfield, Virginia 22161

LASER DOPPLER VELOCIMETER SYSTEM FOR TURBINE STATOR CASCADE STUDIES AND ANALYSIS OF STATISTICAL BIASING ERRORS

by Richard G. Seasholtz

Lewis Research Center

SUMMARY

A laser Doppler velocimeter (LDV) built for use in the Lewis Research Center's turbine stator cascade facilities is described. The signal processing and self-contained data processing are based on a computing counter. A procedure is given for mode matching the laser to the probe volume. An analysis is presented of biasing errors that were observed in turbulent flow when the mean flow was not normal to the fringes. It is shown that significant errors can result in LDV data taken in turbulent flow when the fringe normals are more than about 20° from the mean flow direction. This error is in addition to the previously reported error that occurs even for mean flow parallel to the fringe normals and is a function of the optical parameters of the LDV, the system gain, and the optical properties and size distribution of the scattering centers, as well as the turbulence intensity. The analysis presented in this report satisfactorily explains the biasing observed in the 81-centimeter-diameter turbine stator cascade facility. Data taken in a turbulent free jet, which further confirms the analysis, are also presented.

INTRODUCTION

The laser Doppler velocimeter (LDV) is a useful new instrument for studying a wide variety of flows. Its ability to map flow fields without disturbing the flow makes it an ideal instrument for use in turbine and compressor research for advanced airbreathing engines. The LDV is particularly attractive for studies of transonic and supersonic flow designs where it is difficult to use conventional diagnostic techniques, such as hot wire probes and pressure probes, to accurately measure flow properties without altering the flow under study. Since the first reported LDV (ref. 1), much work has been conducted. (See, e.g., ref. 2.) An example of the use of an LDV for aircraft turbomachinery studies is the mapping of flow in a low-speed compressor (ref. 3).

This report describes the LDV system built for use in the Lewis Research Center's 81-centimeter (32-in.) diameter and 51-centimeter (20-in.) diameter annular turbine stator cascade facilities. (Reference 4 reports the results obtained with this instrument in the 81-cm-diam. cascade facility. Preliminary results for this system were also presented in ref. 5.) The LDV system was designed to measure flow velocities in the transonic range (up to 350 m/sec). The optical system is of the dual scatter type and has off-axis collection of the scattered light. The plane of the two incident beams may be rotated remotely to permit the measurement of any velocity component normal to the direction of the input beams.

The electronics system is based on a commercial computing counter and directly measures the Doppler frequency (over a range of 10 to 80 MHz). The computing counter is used for data reduction so that the LDV data processing is self-contained and does not rely on external computing facilities. The mean velocity and turbulence intensity can be measured on a point-by-point basis or one component of the mean velocity can be continuously plotted as a function of position.

Particular emphasis is given in this report to two important factors that were crucial in the design and operation of this LDV system. First, it is shown that measurement errors caused by gradients in the fringe spacing can be minimized by a mode-matching procedure. The details of this procedure are presented. Second, an analysis is presented of a new statistical biasing effect that was observed during the study of the 81-centimeter-diameter turbine cascade of reference 4. This biasing is significant in turbulent flow (as in a stator wake) when measuring mean velocity components at angles more than 20° from the average flow direction. The reason for this biasing is that the instantaneous rate of velocity measurements is dependent on the angle between the instantaneous flow direction and the orientation of the fringes in the probe volume. In the calculation of statistical quantities, such as mean velocity and standard deviation, this dependence causes bias by weighting states of flow with a higher measurement rate more heavily than those with a lower measurement rate.

Statistical biasing has been described in reference 6 for a mean flow normal to the fringes. In this report a more general analysis is presented for isotropic turbulent flow with mean flow at any angle from the fringe normals.

LDV OPTICAL SYSTEM

The LDV optical system uses the conventional dual scatter technique (ref. 7) with off-axis collection of the scattered light. The laser and all optical components are mounted on a rigid plate (fig. 1) that can be moved by a traversing mechanism to survey the test region. (See ref. 4 for details on the traversing mechanism used for the 81-cm-diam. cascade study.)

The argon-ion laser has an intracavity etalon and an output power of about 1 watt in a vertically polarized, single axial, transverse-electromagnetic (TEM_{00}) mode at a wavelength of 0.5145 micrometer. As shown in figure 1 the beam is divided into two equal power parallel beams by an appropriately coated optical flat (12.7 mm thick). The separation of the parallel beams is about 1 centimeter.

A Dove prism is used as an image rotator to rotate the pair of beams about their midpoint. The prism is mounted and alined within a remotely controlled rotary actuator so that the two output beams trace a common circular path as the prism rotates. This feature allows the measurement of any velocity component lying in the plane normal to the incident beams.

The focusing lens is chosen to have a focal length compatible with the dimensions of the test region under study (e.g., a simple planoconvex lens with a 127-mm focal length was used in ref. 4).

The receiving optics consist of a pair of doublets corrected for spherical aberration (for an object-to-image ratio of infinity). (In ref. 4 50-mm-diam., 200-mm-focal-length lenses were used.) Their axis is positioned about 20° from the backscatter direction to minimize the amount of stray scattered light from the inner wall of the test region reaching the receiving optics. The off-axis receiving optics limit the length of the probe volume (region where velocity is measured), thus giving better resolution in the direction of the incident beams. A pinhole aperture is used at the image point of the probe volume in front of the photomultiplier (type 8645) to define the effective probe volume length and to prevent stray light from entering the photomultiplier tube. (In the system for the 81-cm-diam. cascade, a 0.35-mm-diam. pinhole limited the effective probe volume length to 0.8 mm.)

The two beams that cross to form the probe volume fringes must have two properties. First, their diameter at the probe volume must be fixed to give the correct number of fringes required by the LDV signal processor. (Ten fringes are needed for the processor used in this system.) Too few fringes will result in no output and too many fringes will waste the available laser power with an attendant reduction in the Doppler signal-to-noise ratio. Second, the beam waists (positions of minimum beam diameters) must be at the crossing point. If this condition is not met, the fringe spacing gradient may be sufficiently large to give significant errors in velocity measurements based on the assumption of uniformly spaced fringes. The fringe spacing s for intersecting plane waves is

$$s = \frac{\lambda}{2 \sin \frac{\theta}{2}} \tag{1}$$

where λ is the wavelength of the light and θ is the angle between the two beams. (All symbols are defined in appendix A.) However, as shown in reference 8 the fringe spacing is not uniform along the probe volume length for spherical converging or diverging wavefronts. The gradient in the fringe spacing is approximately

$$\frac{ds}{dz} = \frac{s}{R} \tag{2}$$

where R is the radius of curvature of the wavefront and z is the coordinate along the bisector of the beams. The wavefront curvature of a Gaussian beam (output of laser operating in a TEM_{00} mode) is infinite (i.e., a plane wave) only at the beam waist; away from the waist the wavefront is approximately spherical and is given by (ref. 9)

$$R = z' \left[1 + \left(\frac{\pi w_o^2}{\lambda z'} \right)^2 \right] \tag{3}$$

where w_o is the radius of the beam waist (beam radius is defined as radial distance from beam axis to point where the intensity is $1/e^2$ of its value at the center of the beam), and z' is the distance from the waist measured along the beam axis. Thus, in general, the fringe spacing is not constant for fringes formed by crossed Gaussian beams. The case where the beam waists are located before the crossing point is shown in figure 2. The wavefront curvature in the probe volume is then positive so the fringe spacing increases in the z direction. Examination of equation (2) shows that the fringe spacing gradient becomes smaller as the radius of curvature of the wavefront becomes larger. Thus, placing the beam waists at the cross point minimizes the gradient (and resulting errors in the LDV velocity measurements).

To satisfy these two conditions (proper beam waist positions and diameters), additional lenses (or possibly a single lens) are needed between the laser and the focusing lens. The procedure used to calculate the positions and focal lengths of these lenses is given in appendix B.

LDV SIGNAL PROCESSING SYSTEM

The function of the LDV signal processing system is to measure the Doppler frequency (which is proportional to the velocity of the particle passing through the probe volume) of the Doppler burst from the photomultiplier tube. These bursts occur randomly at an average rate that is determined by the concentration of seed particles, which

may be either naturally occurring or artifically introduced into the flow. Usually seed material, such as silicone oil droplets or aluminum oxide particles, is used to increase the data rate and to control the particle size distribution. Even with artificial seeding the Doppler bursts rarely overlap, so each may be treated independently. Because of the spread in particle sizes and because of the random nature of the individual particle trajectories, the amplitudes of the Doppler bursts are random with widely varying signal-to-noise ratios.

In principle, a single Doppler frequency measurement gives the instantaneous velocity at a point. However, actual Doppler bursts may have a low signal-to-noise ratio, which causes random errors in the measured velocities. Furthermore, for a turbulent flow, the actual instantaneous velocities will be varying in a random manner. Thus many measurements (often 1000 or more) are taken and used to calculate statistical parameters, such as mean velocity and standard deviation.

For a steady flow the standard deviation is only a result of noise in the signal or random errors in the measurement process. For a fluctuating flow, however, the standard deviation is a result of both noise and actual flow fluctuations. Thus, it is necessary to have the fluctuations due to noise be much less than the actual flow fluctuations if the standard deviation of the measurements is to be identified with the turbulence intensity. The processing of these many individual measurements is one of the most important considerations in designing an LDV system.

The approach taken in this system was to include the data processing in the system rather than to record all the data for later reduction in external computing facilities. A commercial computing counter was chosen as the basis for the LDV signal processor and data processing system because of its high-accuracy (±1 ns) time-interval measurements, as well as its computing ability. (The Doppler frequency is found by measuring the time interval corresponding to a fixed number of Doppler cycles.)

However, the computing counter cannot directly use the signal from the photomultiplier tube because of the random nature of the signal and because of the large number of low-amplitude bursts with poor signal-to-noise ratios. The signal from the photomultiplier tube must first be conditioned to provide a standardized signal to the computing counter as well as to eliminate any signals that do not result from valid Doppler bursts.

The circuitry built to provide these functions is described in appendix C. This signal processor converts the Doppler burst from the photomultiplier tube to a single-cycle square wave, eight Doppler periods long, whose period is measured by the computing counter. It also provides a validation check by requiring that the Doppler burst have at least 10 consecutive cycles with amplitudes greater than a preset threshold. Furthermore, it eliminates signals with amplitudes greater than another preset level, which allows a reduction in the number of velocity measurements of large particles, which may not accurately follow the flow. The input Doppler frequency range of the signal processor is 10 to 80 megahertz.

DATA PROCESSING

The data rate (rate of valid velocity measurements) is limited by the computing counter's measurement cycle time to about 1500 measurements per second. This rate, although low compared with the maximum data rate of some LDV processors, which may exceed 500 000 measurements per second, still requires on-line data processing to reduce the amount of data to be recorded. The computing counter's associated programmer provides a convenient, versatile means for processing the raw velocity and probe volume position data; however, the usable data rate is further limited by the programmer's speed to about 100 to 200 measurements per second, depending on the actual number of steps in the program. The processed data may be presented on the computing counter's digital display, or it may be recorded on either an X-Y recorder or a digital recorder. (See the system block diagram in fig. 3.)

Two types of programmed data processing procedures are used. One, a point by point procedure, requires that the probe volume remain at a fixed position until a preset number (typically 1000) of velocity measurements are taken. These data are checked and any wildly erroneous data, usually less than 0.1 percent of the total number, are rejected. (The criterion used in ref. 4 was to reject data more than three standard deviations from the mean.) Statistical parameters (e.g., mean velocity, standard deviation, and coefficient of skewness) are then calculated from the remaining data. This procedure is repeated for other fringe pattern orientations to get data for other velocity components so that velocity magnitude and flow angle can be calculated.

The second data processing procedure involves continuously moving the probe volume through the test region. The fringe orientation remains fixed and a running average is computed for the mean value of the corresponding velocity component. This scan can be repeated for a second fringe orientation. The advantage of the continuous scan method over the point by point method is the greatly reduced data taking time, although only mean velocities are obtained. The continuous scan rate for the work reported in reference 4 was about 0.023 centimeter per second. Details of the data processing procedures used in the 81-centimeter-diameter turbine stator cascade study are given in reference 4.

STATISTICAL BIASING ERRORS IN LDV MEASUREMENTS IN TURBULENT FLOW

Causes of Statistical Biasing Errors

Although the LDV is capable of accurately measuring the velocity of an individual scattering center as it passes through the probe volume, in turbulent flow errors can occur in calculating statistical quantities, such as mean velocity and standard deviation.

These errors, called biasing errors, occur when attempting to calculate time-average statistical parameters from the velocity distribution constructed from a large number of individual measurements. A simplified explanation of this biasing phenomenon will first be given to illustrate the physics of the problem. This is followed by a general analysis for isotropic turbulent flow and, finally, by a comparison with experimental data taken in a free turbulent jet.

The fringe pattern formed in an LDV probe volume (see fig. 4) ideally consists of plane parallel fringes oriented with their normals parallel to the plane defined by the two incident beams and perpendicular to the bisector of the two beams. The intensity of the bright fringes decreases in the radial direction with a Gaussian envelope (see fig. 5).

Consider a two-dimensional incompressible flow passing through the probe volume (i.e., the flow is in the x-y plane). Assume the fluid is uniformly seeded with identical particles. (Their number density n_p is assumed to be small so that, at most, only one particle will be in the probe volume at any time.) As a particle passes through the fringe pattern, the scattered light is detected and is converted to an electrical signal called a Doppler burst. This signal has a waveform that corresponds to the fringe pattern crossed by the particle; the amplitude of the signal during the Doppler burst is assumed to be proportional to the intensity at each point on the particle's trajectory. The frequency at which the particle crosses the fringes is proportional to the particle's velocity and is found by measuring the time required for the particle to cross a fixed number of fringes.

In this discussion a model of the signal processor is used that requires the amplitude of each cycle of the electrical signal during the Doppler burst to be above some fixed level (threshold) in order to achieve a valid velocity measurement. (The low-frequency part of the signal (pedestal) is removed before the signal reaches the level detector, but, since the amplitude of the high-frequency component is proportional to the amplitude of the total signal, this step may be neglected in this discussion.) Various techniques are used in the signal processor to eliminate signals where this condition is not met.

In figure 5 it can be seen that the envelope of the fringe intensity (and hence the electrical signal amplitude) depends only on the radial distance from the center of the probe volume in the x-y plane. Each cycle of the signal must be above some fixed level for some minimum number of cycles. The path length needed for the particle to cross this number of fringes increases as the angle φ between the particle trajectory and the fringe normals increases. Thus the intensity of the fringe envelope at the end points of a path crossing a fixed number of fringes N decreases as φ increases. Since it is required that each cycle be above a fixed level, there exists a maximum value of φ beyond which it is impossible to obtain a velocity measurement. (The case of $\varphi = 90^{\circ}$ will result in a signal with only the envelope as no fringes will be crossed regardless of the particle's path length.) Furthermore, as shown in figure 5, there exists a maximum distance p, equal to the distance of closest approach of the particle to the center of the

probe volume that can result in a velocity measurement. This maximum permissible distance of closest approach is a function of the angle φ between the flow direction and fringe normals (as φ increases p decreases).

The rate of velocity measurements ν is given by the velocity of the particles times their number density times the cross section area (see fig. 5) normal to the flow that will give velocity measurements, that is,

$$\nu = Vn_p(2pL) \tag{4}$$

where L is the length of the probe volume. Here, to simplify the analysis, it is assumed that the probe volume is a cylinder of length L rather than an ellipsoid (see fig. 4). If desired, the true ellipsoidal shape may be incorporated by slicing the probe volume into several sections and repeating the analysis for each section. Since p is a function of the φ, it follows that the rate of velocity measurements is also a function of φ; the rate of measurements decreases as φ increases.

If the flow is turbulent, the velocity magnitude and flow angle vary in a random manner. To calculate valid statistical quantities from the large number of measurements (measurements with V and φ varying) the rate of measurements must be independent of V and φ, which clearly is not the case. A dependence of the data rate on the velocity magnitude or angle will cause averages calculated from these velocity measurements (each measurement being equally weighted) to be different than time-average quantities. (Time averages, as would be given by equally weighted velocity measurements taken at a constant rate, are the quantities wanted in most flow measurements.) Examination of equation (4) shows that two things can affect the data rate.

First, the rate of measurements is proportional to the velocity magnitude. This results in a measured velocity distribution that is biased in favor of higher velocity. The measured mean velocity is larger than the true time-averaged velocity due to this effect, and the error is on the order of the square of the turbulence intensity. This biasing effect is discussed in reference 6.

Second, the rate of measurement varies with the angle φ (because p is a function of φ). This becomes important when the angle between the fringe normals and the flow direction is large (e.g., for $\varphi \geq 20^{\circ}$), and causes the measurement rate to be larger for smaller φ. Thus the distribution constructed from these measurements is weighted in favor of velocity fluctuations that cause the flow to be closer to the fringe normals. This effect also results in a measured value of the mean velocity component that is larger than the true time-averaged velocity component.

This can be seen by considering a simple example: a flow that has only two states. Each state has the same velocity magnitude V, but different flow angles with $\varphi_1 < \varphi_2$. Equal time is spent in each state so that the mean velocity component measured is

$$V_{meas} = V\left(\frac{\nu_1 \cos \varphi_1 + \nu_2 \cos \varphi_2}{\nu_1 + \nu_2}\right) \tag{5}$$

It is obvious that V_{meas} is dependent on the values of ν_1 and ν_2, which are functions of the flow angle. The unbiased value of V_{meas} is found only when the measurement rate is independent of the flow angle so that $\nu_1 = \nu_2$. Since, $\nu_1 > \nu_2$ for $\varphi_1 < \varphi_2$, the biased value of V_{meas} will be greater than the unbiased value.

A common technique in making LDV measurements in flows where the flow direction is not a priori known is to measure two orthogonal velocity components from which the velocity magnitude and flow angle are calculated. At least one of these components will be more than 45^o from the flow angle and will have a large error if the flow is turbulent, which will lead to a large error in the calculated velocity magnitude. Furthermore, if the two components do not happen to be at $\pm 45^o$ from the mean flow direction, the computed flow angle will also be in error.

In the next section this angle biasing is analysed for isotropic turbulent flow with an arbitrary particle size distribution. The actual error will be shown to be a function of the Gaussian beam parameters in the probe volume, the gain of the electronics, the optical properties and size distribution of the scattering centers, and the turbulence intensity, as well as the angle between the mean flow direction and the fringe normals.

Analysis

In this section the fringe model of the dual beam LDV is used (ref. 7). A TEM_{00} laser beam of power P_l and wavelength λ is divided into two equal power parts, which are focused so they cross at their waists (see appendix B). The radius of each waist at the $1/e^2$ intensity points is w_o, and the crossing angle is θ. These four parameters, P_l, λ, w_o, and θ, completely specify the fringes that make up the probe volume. The actual intensity distribution of the fringes (see fig. 4) is a three-dimensional function of the beam parameters (ref. 7). (The constant fringe intensity envelope is an ellipsoid with length-to-width ratio $\sim 1/\theta$.) Here, it is assumed that the fringe intensity is constant along the z-axis. This is a reasonable assumption for small θ and off-axis receiving optics, where the receiving optics determine the length of the probe volume actually used.

The fringe spacing s is given by

$$s = \frac{\lambda}{2 \sin \frac{\theta}{2}} \tag{1}$$

The number of fringes N within the waist diameter is

$$N = \frac{2w_o}{s} \tag{6}$$

The spatial variation of the fringe intensity is given by

$$I(x, y) = I(r)\left[1 + \cos\frac{2\pi x}{s}\right] \tag{7}$$

where

$$I(r) = \frac{2P_l}{\pi c w_o^2} e^{-2(r/w_o)^2} \tag{8}$$

is the mean intensity of light in the probe volume and

$$r = (x^2 + y^2)^{1/2} \tag{9}$$

is the radial coordinate. (In this report intensity is defined as time-average radiant-energy density (in J/m^3). Thus the velocity of light c times the integral of I(r) over the cross section of the beam is equal to the laser power P_l.)

The model used for the flow is two-dimensional incompressible flow with a Maxwellian velocity distribution

$$f(u,v) = \frac{1}{2\pi\sigma_v^2} \exp\left\{-\frac{(u - u_o)^2 + (v - v_o)^2}{2\sigma_v^2}\right\} \tag{10}$$

Here u and v are the velocity components along the x and y directions. This can be written in polar coordinates using the transformations

$$\begin{aligned} u &= V\cos\varphi \\ v &= V\sin\varphi \end{aligned} \tag{11}$$

to find

$$f(V, \varphi) = \frac{1}{2\pi\sigma_v^2} \exp \left\{ - \frac{(V - V_o)^2 + 2VV_o \left[1 - \cos (\varphi - \varphi_o)\right]}{2\sigma_v^2} \right\} \varphi \tag{12}$$

Here V_o is the magnitude of the mean velocity and φ_o is the angle between the mean velocity and the fringe normals. The randomly fluctuating quantities V and φ are similarly defined. The turbulence is assumed to be isotropic with a turbulence intensity σ_v/V_o.

The scattering particles are assumed to have a uniform number density n_p and a normal size distribution

$$f(a) = \frac{n_p}{\sqrt{2\pi}\,\sigma_a} e^{-(a-a_o)^2/2\sigma_a^2} \tag{13}$$

where a_o is the mean diameter and σ_a is the diameter standard deviation. The fact that this distribution gives negative diameters for some particles does not matter here because only that part of the distribution having particles with diameters larger than some fixed positive diameter will be used.

It is also assumed that the particles follow the flow and that the particle velocity and size are statistically independent so a joint distribution may be defined as

$$f(V, \varphi, a) = f(V, \varphi) f(a) \tag{14}$$

where $f(V, \varphi, a)\, V dV d\varphi da$ is the number density of particles with V, φ, and a in the ranges V to $V + dV$, φ to $\varphi + d\varphi$, a to $a + da$. The rate at which the particles simultaneously in these ranges pass through a cylinder (with its axis normal to the flow) of length L and radius p is

$$d\nu = V2pL \cdot f(V, \varphi, a) V \, dV \, d\varphi \, da \tag{15}$$

The rate at which particles of all sizes and velocities pass through the cylinder is

$$\nu = \int_0^\infty \int_0^{2\pi} \int_0^\infty V2pL \cdot f(V, \varphi, a) V \, dV \, d\varphi \, da \tag{16}$$

Since φ is the angle of the flow velocity measured from the fringe normals (x direction) the mean value of the component of V normal to the fringes (the velocity measured by an LDV) is

$$\langle |V \cos \varphi| \rangle = \frac{1}{\nu} \int_0^{\infty} \int_0^{2\pi} \int_0^{\infty} |V \cos \varphi| \cdot V2pL \cdot f(V, \varphi, a) V \, dV \, d\varphi \, da \qquad (17)$$

where the absolute value of the velocity component is used because the LDV cannot determine flow direction. The question that must be answered is whether this differs from the true value of the component of the mean velocity, $v_0 \cos \varphi_0$, and if so, what is the error.

In order to evaluate the integrals in equations (16) and (17), it is necessary to know the value of p, which is the radius of a cylinder through which pass the particles that result in velocity measurements. It will be shown that p is a function of both the particle size and the angle between the flow direction and fringe normals. This is a consequence of the Gaussian intensity profile of the incident light, the variation of the intensity of the scattered light with particle size, and the principle of operation of LDV counter type of processer. These factors will now be examined.

This analysis is restricted to the counter type of LDV signal processor, which is the most common type used in high-speed gas flows with low-seed-number densities. The analysis specifically applies to the processor described in appendix C; however, the results of the analysis should be qualitatively similar for other counter type of processors (such as those using 4/8 or 5/8 ratio tests for rejection of false measurements).

A typical signal (Doppler burst) from the photomultiplier tube is proportional to the fringe intensity profile shown in figure 5. The amplitude of the signal is proportional to the intensity of the fringes as given by equation (7). The signal is then filtered to remove the low-frequency pedestal, and the resulting signal is applied to a threshold detector. Here it is assumed that a valid velocity measurement results only from a Doppler burst having at least N_{min} cycles above the level of the threshold detector. Typically, $N_{min} = 10$, as for the signal processor described in this report. The Doppler frequency is found by measuring the time between zero crossings for some fixed number of cycles (less than or equal to N_{min}) within the Doppler burst (usually eight cycles).

Note that, as the angle between the flow velocity and the fringe normals increase toward 90°, fewer fringes will be crossed and that at some angle there will be less than N_{min} cycles in the Doppler burst above the threshold. For the purposes of this analysis the threshold for a valid Doppler signal will be defined in terms of the equivalent amount of power scattered into the receiving optics; this equivalent power is denoted P_{thres}. (The actual value of P_{thres} is a function the photomultiplier tube gain and quantum efficiency, the photomultiplier tube load resistor, the gain of any amplifiers in the system, and the actual voltage threshold of the signal processor.) The power scattered into the receiving optics is

$$P_s = I(r) c \sigma(a) \Omega \qquad (18)$$

where $I(r)$ is the intensity of the incident light at the location of the particle, and $\sigma(a)$ is the scattering cross section of the particle, which is the power scattered into unit solid angle per unit incident irradiance. In general $\sigma(a)$ is a function of the particle diameter and index of refraction, the scattering angle, and the wavelength of the light, and must be calculated using Mie scattering theory (ref. 10). The solid angle of the receiving optics is Ω. For a given receiving optical system and specified P_{thres} the minimum intensity at a particle needed to trigger the signal processor is

$$I_{thres} = \frac{P_{thres}}{c\sigma(a)\Omega} \tag{19}$$

This threshold intensity occurs at a radius r_{thres} on the envelope of the fringe intensity pattern. For the purpose of determining r_{thres}, the detailed structure of the fringe pattern is neglected; that is, it is assumed that if the particle traverses a distance Δx along the x direction between the two points where it crosses the $r = r_{thres}$ circle, the number of cycles above threshold is $\Delta x/s$ (see fig. 5).

Using equations (8) and (18), the radius at which the power scattered into the receiving optics is equal to P_{thres} is

$$r_{thres} = \left[\frac{w_o^2}{2} \ln\left(\frac{2P_l\Omega\sigma(a)}{P_{thres}\pi w_o^2}\right)\right]^{1/2} \tag{20}$$

The trajectory of a particle passing through the probe volume can be specified by the angle φ made with the direction of the fringe normals and by the distance of closest approach p' to the axis of the probe volume (z axis). The number of fringes crossed by the particle between the points where it crosses the circle with radius r_{thres} is

$$N = \frac{2\cos\varphi}{s}\left(r_{thres}^2 - p'^2\right)^{1/2} \tag{21}$$

The number of cycles in the Doppler burst above the threshold decreases as p' increases and as φ increases.

The maximum value of p' that will result in a Doppler burst with at least N_{min} cycles above threshold is

$$p = \left[r_{thres}^2 - \left(\frac{sN_{min}}{2\cos\varphi}\right)^2\right]^{1/2} \tag{22}$$

Using equation (20) in equation (22) gives p (which is the maximum value of p' that will result in a valid measurement) as a function of the particle size a and the angle φ.

$$p(a, \varphi) = \left[\frac{w_o^2}{2} \ln\left(\frac{2P_l \Omega \sigma(a)}{P_{thres} \pi w_o^2} \right) - \left(\frac{sN_{min}}{2 \cos \varphi} \right)^2 \right]^{1/2} \tag{23}$$

This expression for p is used in the integrals for ν and $\langle V \cos \varphi \rangle$ (eqs. (16) and (17)), which become

$$\nu = 2L \int_0^{2\pi} \int_{a_{min}(\varphi)}^{\infty} \int_0^{\infty} V^2 p(a, \varphi) f(V, \varphi) f(a) \, dV \, da \, d\varphi \tag{24}$$

$$\left\langle |V \cos \varphi| \right\rangle = \frac{2L}{\nu} \int_0^{2\pi} \int_{a_{min}(\varphi)}^{\infty} \int_0^{\infty} V^3 |\cos \varphi| p(a, \varphi) f(V, \varphi) f(a) \, dV \, da \, d\varphi \tag{25}$$

The lower limit on the integration over the particle diameter a is $a_{min}(\varphi)$, which is the diameter of the smallest particle passing through the center of the probe volume (at the angle φ) that will give a measurement. To find a_{min} set $p(a, \varphi) = 0$ in equation (23) and solve for $a_{min}(\varphi)$. This is difficult because the scattering cross section $\sigma(a)$ is not a simple function. To simplify the evaluation of $\sigma(a)$ an exponential approximation

$$\sigma(a) \cong \sigma_o e^{\mathscr{A}a - \mathscr{B}} \tag{26}$$

is used (because of the form of eq. (23)) where $\mathscr{A}$ and $\mathscr{B}$ are chosen to approximate the actual cross section for the particle size range and scattering angle of interest, and $\sigma_o = 1$ square meter. For example, figure 6 shows $\sigma(a)$ for backscatter, a refractive index of 1.4 (silicone oil), and a wavelength of 0.5145 micrometer, which parameters are similar to those of the LDV system described in this report. For this example equation (26) with $\mathscr{A} = 2.96 \times 10^6$ meter^{-1} and $\mathscr{B} = 34.07$ (shown as a dashed line in fig. 6) gives a reasonable fit over the size range of interest here (0.5 to 2.0 μm). Use of the actual cross section would present difficulties since $\sigma(a)$ is a rather complex function of the particle size and scattering angle. Using this approximation in equation (23) allows equation (20) for p to be rewritten:

$$p(a, \varphi) = \left\{ \frac{w_o^2}{2} \left[\mathscr{A}a - \mathscr{B} + \ln\left(\frac{2P_l \Omega \sigma_o}{P_{thres} \pi w_o^2} \right) \right] - \left(\frac{sN_{min}}{2 \cos \varphi} \right)^2 \right\}^{1/2} \tag{27}$$

Setting $p = 0$ gives an expression for $a_{min}(\varphi)$:

$$a_{min}(\varphi) = \frac{1}{\mathscr{A}} \left[\mathscr{B} + \frac{1}{2} \left(\frac{sN_{min}}{w_o \cos \varphi} \right)^2 - \ln\left(\frac{2P_l \Omega \sigma_o}{P_{thres} \pi w_o^2} \right) \right] \tag{28}$$

Equations (24) and (25) may now be evaluated using equations (11), (13), (27), and (28). This evaluation has been carried out using numerical techniques for the parameters relevent to the LDV system discussed earlier in this report.

Theoretical Results

In this section the effects of turbulence intensity, particle size distribution, and threshold sensitivity on angle biasing error are shown. All the calculations were made using these parameters: waist radius of input beams, 62.5 micrometers; fringe spacing, 6.25 micrometers; solid angle of scattered light intercepted by receiving optics, Ω = 0.05 steradian; scattering cross section, $\sigma(a) = \sigma_o \exp(\mathscr{A}a - \mathscr{B})$ square meters, with σ_o = 1 square meter, $\mathscr{A} = 2.96 \times 10^6$ reciprocal meters, and $\mathscr{B} = 34.07$, as shown in figure 6; wavelength, λ = 0.5145 micrometer; and the required minimum number of Doppler cycles with amplitude above threshold, $N_{min} = 10$. For these parameters equation (28) gives $a_{min}(0) = 0.858$ micrometer, which is the smallest particle that will give a valid measurement. Thus, for particle size distributions with mean diameters smaller than this, the particles being used come from the tail of the distribution curve.

Figure 7 shows the error in the measurement of the velocity component as a function of φ_o for a monodisperse particle size distribution (all particles having same size). The error is defined as

$$\text{error} = \frac{\langle | V \cos \varphi | \rangle}{| V_o \cos \varphi_o |} - 1 \times 100 \text{ percent} \tag{29}$$

This figure shows that the error decreases as the particle size increases. This is because larger particles can give valid velocity measurements for larger values of φ, which results in more equal weighting of velocity fluctuations on each side of φ_o. Also note that the error at $\varphi_o = 0$ is about 1 percent regardless of the particle size. This

error is due to the variation of particle flux through the probe volume as a function of velocity as discussed in reference 6.

Figure 8 shows how polydisperse particle size distributions (particles having different sizes) affect the angle biasing error. As one would expect from the data shown in figure 7, an increase in the standard deviation of the particle size distribution tends to decrease the biasing error. Of course, in most LDV systems it is not desirable to use large particles or particles having a broad size distribution because of possible lag between the particle velocity and the flow velocity. For aerodynamic studies in compressors and turbines, it has been shown (refs. 11 and 12) that the particle diameter should be about 1 micrometer or less.

The effect of the system sensitivity, or gain, on the angle biasing is shown in figure 9. A decrease in the ratio of the trigger threshold power to incident power, which can result from increasing either the system gain or the laser power, will reduce the error. This shows that the LDV system should be operated at the highest gain and laser power possible without introducing excessive noise (which would also cause erroneous measurements).

Finally, the variation of angle biasing error with turbulence intensity is shown in figure 10. For the parameters used for this figure, significant error is found at $\varphi_0 = 45^\circ$ for turbulence intensities greater than 5 percent. Note again that the error at $\varphi_0 = 0$ is approximately the square of the turbulence intensity.

Comparison of Theory with Experimental Results

The motivation for the above work was a discrepancy in the results of LDV measurements in a turbine stator cascade facility (ref. 4). The discrepancy noted was a marked difference in the mean velocity magnitude in the wakes of turbine stator vanes calculated from two orthogonal measurements made at approximately $\pm 45^\circ$ from the flow direction as compared with the velocity measured along the flow direction. As shown in reference 4, the theory presented in this report satisfactorily explains the observed data. An additional experiment was performed to check the theory.

A turbulent jet was generated by placing a pair of 1.3-millimeter-diameter wires oriented at right angles in a 7.4-millimeter-inside-diameter tube about 30 millimeters from the tube exit. The intensity of the turbulence at the exit as measured by the LDV system was approximately isotropic ($\sigma_v/V_0 = 10$ percent ± 1 percent over a range of angles, $\varphi_0 = \pm 55^\circ$ from the mean flow direction). The mean flow velocity magnitude V_0 was set at 225 meters per second. The error in the measurement of the mean value of the velocity component was defined as

$$\text{Error} = \left(\frac{\langle V_{meas} \rangle}{|V_o \cos \varphi_o|} - 1 \right) \times 100 \text{ percent} \tag{30}$$

This experimentally measured error is shown in figure 11 for two values of amplifier gain differing by 20 decibels (factor of 10 in voltage gain). The error at $\varphi_o = 0$ is set at 1 percent to agree with the predicted error; that is, the value of V_o used in equation (30) is $0.99 \langle V_{meas} \rangle$ at $\varphi_o = 0$. Also shown in this figure is the calculated value of the error for two values of the ratio P_{thres}/P_l. These two curves also correspond to the same factor of 10 difference in the system gain. The probe volume diameter and fringe spacing are approximately the same for the experimental and calculated data. The particle size distribution (as given by the manufacturer of the particle generator) used in the experiment was also used for the calculated data. The approximate form for the backscatter cross section as given in figure 6 was used for the calculated curve; although, in the experiment, the scattering angle was 150^o rather than 180^o. This makes little difference because it is difficult, in any case, to determine the actual value of the ratio P_{thres}/P_l for an LDV system because of the need to know parameters such as the photomultiplier tube quantum efficiency and gain. However, an estimate for the ratio P_{thres}/P_l, based on typical data for the photomultiplier used, is $P_{thres}/P_l \sim 1 \times 10^{-8}$. This estimate is shown as the dashed curve in figure 11.

Two important observations, based on figure 11, confirm the validity of the analysis of the angle biasing effect. First, the shape of the error verses angle curve for the experimental data agrees well with the theoretical curve. Second, for a factor of 10 change in the system gain (P_{thres}/P_l), the change in the error is about the same for the theoretical and experimental data. The question is then what, if anything, can be done to eliminate, or at least minimize, this error.

The first conclusion that can be reached from these results is that it would be very difficult to apply a correction factor to accurately compensate for angle biasing errors. The reason is that the error is a function of many system parameters that are not easy to determine or that can change with time. For example, the error is a function of the overall system gain, which depends on things like the photomultiplier tube gain and loss of light due to scattering from windows. This difficulty does not occur in attempts to correct the biasing error if the fringe normals are in the flow direction because, in that case, the error is only a function of the turbulence intensity.

Since it does not appear to be feasible to correct data affected with angle biasing, steps must be taken to minimize the error. One measure that will reduce the error is to restrict the angle between the fringe normals and the flow direction. This was done in the work reported in reference 4 where the angles used to calculate the flow angle were $\pm 20^o$ from the expected flow direction. The velocity magnitude calculated from these measurements can be checked by comparing it with the velocity measured in the flow

direction. Of course this approach assumes that the flow direction is approximately known, which may or may not be true.

A second possible solution might be to shift the frequency of one of the input laser beams with a moving diffraction grating or an acousto-optic modulator. (See, for example, ref. 13.) This, in effect, creates a moving fringe pattern in the probe volume. With a moving fringe pattern the velocity measurement rate can be made less sensitive to the angle between the flow direction and the fringe normals. This is possible because the number of cycles in the Doppler burst is a function of the fringe velocity as well as the particle trajectory. For instance, if one of the input beams is shifted in frequency by f_s (which causes the fringes to move along their normals with a velocity $v_f = sf_s$), the number of fringes crossed as a particle with velocity V passes through the probe volume is

$$N_c = \frac{2w_o}{s}\left(\cos\varphi - \frac{v_f}{V}\right) \tag{31}$$

Note that the number of fringes crossed is decreased if the fringes are moving in the flow direction and is increased if the fringes are moving in the opposite direction. Although this analysis did not include the possibility of moving fringes, it appears that the angle biasing error would be significantly reduced for $v_f \geq V$.

CONCLUDING REMARKS

An LDV system developed for the Lewis Research Center's turbine stator cascade facilities has been described. A design procedure that minimizes gradients in the fringe spacing in the probe volume was given. A detailed analysis of biasing errors encountered during the use of the LDV was presented.

Serious errors can result in LDV data taken in turbulent flow when the fringe normals are more than about 20° from the flow direction. This error is in addition to the biasing error discussed in reference 6, which is present even for flow parallel to the fringe normals. The angle biasing error is a function of the optical parameters of the LDV system, the system gain, and the optical properties and size distribution of the scattering centers. In general, the error increases with (1) turbulence intensity, (2) increase in angle between fringe normals and flow, (3) decrease in particle size for

monodisperse particles, (4) decrease in standard deviation of particle size distribution (with fixed mean diameter), and (5) decrease in overall system gain.

Lewis Research Center,
National Aeronautics and Space Administration,
Cleveland, Ohio, September 16, 1976,
505-04.

APPENDIX A

SYMBOLS

A, B, C, D	elements of ABCD matrix, see eq. (A8)
$\mathscr{A}$	parameter in approximation for cross section (see eq. (26)), m^{-1}
a	particle diameter, m
a_{min}	minimum particle diameter that can result in velocity measurement, m
$\mathscr{B}$	parameter in approximation for cross section (see eq. (26))
c	velocity of light, 2.998×10^8 m/s
d	separation between beams at focusing lens, m
d_p	diameter of probe volume, m
d_1	distance between waist 1 and mode matching lens, m
d_2	distance between waist 2 and mode matching lens, m
f	focal length of focusing lens, m
f_e	focal length of equivalent thin lens or effective focal length (see appendix A), m
f(a)	particle diameter distribution function, see eq. (13), m^{-4}
f(u, V)	two-dimensional velocity distribution in rectangular coordinates, see eq. (10), s^2/m^2
$f(V, \varphi)$	two-dimensional velocity distribution in polar coordinates, see eq. (12), s^2/m^2
$f(V, \varphi, a)$	joint distribution function, $f(V, \varphi)f(a)$, s^2/m^6
f_D	Doppler frequency, MHz
I(r)	mean intensity of light in probe volume, J/m^3
I(x, y)	intensity of light in probe volume, J/m^3
I_{thres}	intensity of light corresponding to threshold of electronics, J/m^3
L	length of probe volume, m
L_c	cavity length of laser, m
L_e	distance between laser and focusing lens (see fig. 17), m
L_m	distance between waists of modes to be matched (see fig. 16), m

ℓ	distance from equivalent thin lens to beam crossing point, m
N	number of fringes
N_c	number of fringes crossed
N_{min}	minimum number of Doppler cycles needed by electronics
n	index of refraction
n_p	number density of scattering centers (seed particles), m^{-3}
P_ℓ	output power of laser, W
P_s	power of light scattered into receiving optics, W
P_{thres}	value of P_s corresponding to threshold of electronics, W
$p(a, \varphi)$	maximum distance of closest approach to axis of probe volume that will result in valid velocity measurement, m
p'	distance of closest approach to axis of probe volume, m
q	complex radius of Gaussian beam, m
R	wavefront radius of curvature, m
$R_{1,2}$	laser mirror radii, m
r	radial coordinate in probe volume, equal $\sqrt{x^2 + y^2}$, m
r_{thres}	radius in probe volume at which $I(r) = I_{thres}$, m
r_1	ray height at entrance of region, m
r_1'	ray slope at entrance of region
r_2	ray height at exit of region, m
r_2'	ray slope at exit of region
s	fringe spacing, m
T	time equal to eight Doppler periods, s
t	time, s
u	velocity component in x direction, m/s
V	velocity magnitude, m/s
V_{meas}	measured velocity, m/s
v	velocity component in y direction, m/s
$v_\perp$	velocity component perpendicular to fringes, m/s
w	Gaussian beam radius at intensity equal to $1/e^2$ of peak intensity, m

w_o Gaussian beam radius at waist, m

w_{ox} trial value of intermediate beam waist radius, m

w_{pv} Gaussian beam radius at probe volume, m

x coordinate perpendicular to fringes, m

Δx distance in x direction between intersections of particle trajectory with $r = r_{thres}$ circle, m

x_p distance between back surface of focusing lens and beam crossing point, m

x_1 distance between waist 1 and first mode matching lens, see fig. 16(c), m

x_2 distance between waist 2 and second mode matching lens, see fig. 16(c), m

y coordinate perpendicular to axis of probe volume and parallel to fringes, m

z coordinate along axis of probe volume, m

z' coordinate along beam axis, m

z_1 distance between waist and left mirror in laser cavity (see eq. (A12)), m

z_2 $L_c - z_1$, m

θ beam crossing angle

λ wavelength of laser light, m

ν rate of velocity measurements, Hz

$\sigma(a)$ light scattering cross section of particles, m^2

σ_a particle diameter standard deviation, see eq. (13), m

σ_o constant = 1 m^2

σ_v particle velocity standard deviation, see eq. (10), m/s

φ angle between fringe normal and particle velocity

Ω solid angle of light acceptance of receiving optics, sr

Subscript:

o mean value

APPENDIX B

GAUSSIAN BEAM MODE MATCHING FOR LDV OPTICAL SYSTEMS

The basic procedure followed in designing a dual scatter LDV transmitting optical system is usually as follows: First, the diameter d_p of the probe volume is chosen to correspond to the desired transverse spatial resolution. Second, the approximate beam crossing angle θ is chosen, using equation (1), so that the number of fringes $N = 2w_o/s$ within the probe volume is consistent with the requirements of the signal processing equipment. Of course, the Doppler frequency $f_D = v_\perp/s$, where $v_\perp$ is the velocity component perpendicular to the fringes, must also be within the range of the signal processing equipment. Third, the focal length f of the focusing lens is chosen to be the desired distance from the focusing lens to the probe volume. The separation between the input beams is thus $d = 2f \tan(\theta/2)$ as shown in figure 12.

There is an additional requirement that should be satisfied. The beam waists should be at the beam crossing point. This is necessary to minimize gradients in the fringe spacing as discussed in reference 8.

A procedure for getting these desired properties in the probe volume is given in this appendix. An example is then given in which this procedure is applied to a specific LDV system.

Calculation of Beam Crossing Point and Effective Focal Length

After the focusing lens has been selected, the crossing point of the two beams must first be calculated for the given separation d of the parallel input beams (fig. 13). This is done using ray tracing techniques (see, for example, ref. 14) to find the intersection of the central rays of the two beams. This intersection point will not, in general, be at the paraxial focal point because of spherical aberration. The ray trace also gives the crossing angle θ, which, together with the laser wavelength λ, gives the fringe spacing in the plane containing the crossing point. (In general, the fringe spacing will be different in other planes.)

The beam diameters $2w$ at the entrance of the focusing lens are usually small compared with the beam separation d (in fact, $2w/d \sim 1/N$ where N is the number of fringes in probe volume), so the f-number of the beams is large and the paraxial approximation (for rays within each beam) is valid provided the effective focal length at the actual zone the beams pass through is used. Note that, as shown in figure 13, the focal point for these rays does not necessarily coincide with the beam crossing point. A convenient way to visualize this is to consider each section of the lens that a beam passes

through as an equivalent thin prism, to deviate the beam, plus a thin lens with its axis along the centerline of the deviated beam. The focal length of this thin lens will be referred to as the effective focal length f_e. This is shown in the lower part of figure 13. Note that the actual focusing lens shown in the figure is a simple planoconvex lens with the plane surface toward the focal region to minimize spherical aberration, which is undercorrected for this lens (that is, the rim rays focus closer to the lens than do the paraxial rays).

The LDV optics must thus produce a Gaussian beam to the right of the focusing lens that has a waist (with the desired diameter) at the crossing point of the beams. In the next section the theory of Gaussian beams is reviewed. This theory is needed to find the additional optics needed to match the output of the laser to the desired mode in the probe volume.

Properties of Gaussian Beams

The intensity distribution of a Gaussian beam is completely specified, for a given wavelength, by a single parameter - the radius of the beam at its waist. (The beam radius w used here is defined as the distance from the beam axis at which the intensity is $1/e^2$ of the axial intensity.) At the waist the wavefront radius of curvature R is infinite. At points away from the waist the beam radius and wavefront radius of curvature are (ref. 9)

$$w(z') = w_o \left[1 + \left(\frac{\lambda z'}{\pi w_o^2} \right)^2 \right]^{1/2} \tag{B1}$$

$$R(z') = z' \left[1 + \left(\frac{\pi w_o^2}{\lambda z'} \right)^2 \right] \tag{B2}$$

where w_o is the beam radius at the waist and z' is the distance from the waist. The wavefront radius of curvature R is positive for a beam diverging in the positive z' direction.

Another pair of useful equations gives the beam radius at the waist and the position of the waist in terms of the beam radius and wavefront radius of curvature at any point along the beam. These equations, which can be found from equations (B1) and (B2), are

$$w_o = w\left[1 + \left(\frac{\pi w^2}{\lambda R}\right)^2\right]^{-1/2} \tag{B3}$$

$$z' = \frac{1}{R}\left(\frac{\pi w_o w}{\lambda}\right)^2 \tag{B4}$$

The beam radius and wavefront radius of curvature can be combined into a single, complex quantity

$$q(z') = \left[\frac{1}{R(z')} - i\,\frac{\lambda}{\pi w^2(z')}\right]^{-1} \tag{B5}$$

which is called the complex radius of a Gaussian beam (ref. 9). The beam radius and wavefront radius of curvature are then

$$R(z') = \frac{1}{Re\left[\frac{1}{q(z')}\right]} \tag{B6}$$

$$w(z') = \left\{-\frac{\lambda}{\pi\, Im\left[\frac{1}{q(z')}\right]}\right\}^{1/2} \tag{B7}$$

The complex radius is a useful concept because q transforms in the same way as the radius of curvature of a spherical wave (ref. 9). This means the ABCD law can be used to calculate the transformation of Gaussian beams passing through both homogeneous media and lenses.

ABCD Law for Transformation of Gaussian Beams

The ABCD law (ref. 9) relates the value of the complex radius of a Gaussian beam at two points (denoted by subscripts 1 and 2) by the relation

$$q_2 = \frac{Aq_1 + B}{Cq_1 + D} \tag{B8}$$

The matrix with elements A, B, C, and D describes the change in the height r and slope r' of a paraxial ray by

$$\begin{bmatrix} r_2 \\ r_2' \end{bmatrix} = \begin{bmatrix} A & B \\ C & D \end{bmatrix} \begin{bmatrix} r_1 \\ r_1' \end{bmatrix} \tag{B9}$$

Figure 14 shows the geometry and ABCD matrices for the two transformations needed here. One is simply for translation through a homogeneous medium, and the other is the crossing of a spherical interface between two dielectric media.

The ABCD matrices can be cascaded to form a matrix that includes several optical elements. For example, the ABCD matrix for a biconvex thin lens in air with equal radii surfaces ($R_1 = -R$, $R_2 = +R$) and index of refraction n, is given by

$$\begin{bmatrix} A & B \\ C & D \end{bmatrix}_{\text{thin lens}} = \begin{bmatrix} 1 & 0 \\ \frac{1-n}{R} & n \end{bmatrix} \begin{bmatrix} 1 & 0 \\ 0 & 1 \end{bmatrix} \begin{bmatrix} 1 & 0 \\ \frac{1-n}{nR} & \frac{1}{n} \end{bmatrix} = \begin{bmatrix} 1 & 0 \\ -\frac{2(n-1)}{R} & 1 \end{bmatrix} = \begin{bmatrix} 1 & 0 \\ -\frac{1}{f} & 1 \end{bmatrix} \tag{B10}$$

where $f = R/2(n - 1)$ is the focal length of a thin lens. Note that the order of the matrices is the reverse of the order that the beams encountered the various regions and surfaces. Thus the change in the complex radius of a Gaussian beam passing through a thin lens of focal length f is given by equation (B8) as

$$q_2 = \frac{q_1}{1 - \frac{q_1}{f}} \tag{B11}$$

where q_1 is the complex radius of the beam at the entrance of the lens, and q_2 is the complex radius at the exit of the lens.

Gaussian Mode of Laser Cavity

For a laser cavity of length L_c and mirror radii R_1 and R_2 (radii positive as shown in fig. 15), the waist of the TEM_{00} cavity mode (Gaussian mode) is located at a distance (ref. 15)

$$z_1 = \frac{L_c(R_2 - L_c)}{R_1 + R_2 - 2L_c} \tag{B12}$$

from the left hand mirror (z_1 positive to right of mirror 1). The beam radius at the waist is found using equation (B2)

$$w_o = \left[\left(\frac{z_2\lambda}{\pi}\right)^2\left(\frac{R_2}{z_2} - 1\right)\right]^{1/4} \tag{B13}$$

where $z_2 = L_c - z_1$ (z_2 positive to left of mirror 2). This determination of the waist position and beam radius at the waist completely specifies the Gaussian mode within the laser cavity.

The Gaussian mode at the output of the laser is found by applying the ABCD law transformation, described in the preceding section, to the beam passing through the laser output mirror. The ABCD law transformation may also be used to calculate the beam radius and wavefront radius of curvature at the entrance of the focusing lens that will give the Gaussian mode in the region of the probe volume with the desired waist radius and with the waist at the crossing point of the beams. The problem is to match the Gaussian beam from the laser to this mode at the entrance of the focusing lens.

Mode Matching of Gaussian Beams

It is convenient to describe the two Gaussian modes to be matched in terms of the location of their waists and their waist radii. As shown in figure 16, the waist can be either real (as w_{o2} in the mode to the left of the focusing lens), or virtual (as w_{o1} in the mode to the right of the laser output mirror). These modes may be matched by one or more lenses. Techniques for matching with either a single thin lens, or with two thin lenses, are now described.

Mode matching with single thin lens. - Two Gaussian modes can be matched with a single thin lens (ref. 16). If the distance between the two waists (with beam radii w_{o1} and w_{o2}) is L_m, the modes are matched with a thin lens at distance (fig. 16(b))

$$d_1 = \frac{w_{o1}\left(w_{o1}L_m - w_{o2}\left\{L_m^2 + \left[\frac{\pi}{\lambda}\left(w_{o1}^2 - w_{o2}^2\right)\right]^2\right\}^{1/2}\right)}{w_{o1}^2 - w_{o2}^2} \tag{B14}$$

from waist 1. The focal length f of the thin lens is given by

$$\frac{1}{f} = \frac{d_1}{\left(\frac{\pi w_{o1}^2}{\lambda}\right)^2 + d_1^2} + \frac{d_2}{\left(\frac{\pi w_{o2}^2}{\lambda}\right)^2 + d_2^2} \tag{B15}$$

where $d_2 = L_m - d_1$. If f is close to an available focal length and if L_m can be adjusted, it may be possible to achieve a match with a change in L_m. As discussed in reference 16, it is not possible to match all combinations of modes with a single lens. The position of the mode matching lens is where the beam radii are equal. If this position is not between the beam waists a match with a single lens is not possible.

Since mode matching with a single lens requires a unique focal length (for a given L_m), it is often more convenient to use two lenses. With two lenses much more latitude is possible in the choice of focal lengths.

Mode matching with two thin lenses. - Unique focal lengths are not required when mode matching with two lenses.

Figure 16(c) gives the nomenclature used for the positions of the lenses. The distance between the waists of the modes being matched is $L_m = L_1 + L_2$.

The first step is to select two possible lenses having focal lengths f_1 and f_2. Then an intermediate waist radius w_{ox} is selected (a guess). The positions of the two lenses for a mode match are

$$x_{1,2} = f_{1,2}\left\{1 + \frac{w_{o1,o2}}{w_{ox}}\left[1 - \left(\frac{\pi w_{ox} w_{o1,o2}}{\lambda f_{1,2}}\right)^2\right]^{1/2}\right\} \tag{B16}$$

and the distances from waists 1 and 2 to the intermediate waist are

$$L_{1,2} = f_{1,2}\left\{2 + \left(\frac{w_{ox}}{w_{o1,o2}} + \frac{w_{o1,o2}}{w_{ox}}\right)\left[1 - \left(\frac{\pi w_{ox} w_{o1,o2}}{\lambda f_{1,2}}\right)^2\right]^{1/2}\right\} \tag{B17}$$

Equations (B16) and (B17) were found by matching the ABCD coefficients for the transformation between two waists with the ABCD coefficients of a system made up from a thin lens with distances $x_{1,2}$ before and $L_{1,2} - x_{1,2}$ after. The distance $L_m = L_1 + L_2$ between waists 1 and 2 is then a function of the intermediate waist radius w_{ox}. By using an iterative procedure of varying w_{ox} and calculating L_m, one can determine if it is possible to use lenses with the selected focal lengths to achieve a mode match at an acceptable value of L_m. This process can be repeated for other pairs of focal lengths

until an acceptable combination of lens positions and distance between waists 1 and 2 is found.

This mode matching procedure using two thin lenses is useful when it is not convenient to use the single thin lens mode match. An example using the above procedure for a given LDV optical system is given in the next section.

Example of Mode Matching an LDV System

Consider the LDV optical system shown in figure 17. Assume that the beam dividing optics give equal optical path lengths for the two beams and that the distance L_e between the laser output reflector and the focusing lens is adjusted to include any additional optical path length due to the beam dividing optics.

The paraxial focal length of the focusing lens is 12.70 centimeters, so the approximate beam crossing angle θ is 0.079 radians (4.5^o). Suppose about 20 fringes are needed (between $1/e^2$ intensity points); setting the probe-volume beam-waist radius w_{pv} equal to 62.5 micrometers gives the desired number of fringes. (The actual number of fringes by equations (1) and (6) is 19.2.)

Tracing the central rays of the two beams gives the crossing point (measured from the plane surface of the lens) x_p of 12.01 centimeters, and the actual crossing angle θ of 0.07892 radians (4.522^o). The distance, measured along the beam path, from the equivalent thin lens to the crossing point is thus $\ell = 1/(2 \sin(\theta/2)) = 12.67$ centimeters (see also fig. 13). The focal length of the equivalent thin lens is found by tracing the two rays entering the focusing lens at 0.501 centimeter and at 0.499 centimeter from the axis; this gives $f_e = 12.60$ centimeters.

The Gaussian beam at the left of the equivalent thin lens that gives a beam to the right of the lens with a waist radius of 62.5 micrometers at 12.67 centimeters from the lens is found using the appropriate ABCD transformations. Equations (B3) and (B4) then give the location of the waist (14.55 cm to left of focusing lens) and its radius (330.01 μm).

The waist of the laser cavity mode is at the plane mirror (by eq. (B12)) and has a radius of 536.87 micrometers (by eq. (B13)). Again, use of the ABCD transformations and equation (B6) gives the virtual waist location (119.25 cm to left of plane surface of laser output mirror) and radius of waist (465.86 μm).

Suppose the required distance L_e is 120 centimeters. Then the distance between the two waists of the modes to be matched is 120 + 119.25 - 14.55 = 224.70 centimeters. These modes may be matched with either a single thin lens, or with two thin lenses. (One can compensate for the finite thickness of the lenses by adjusting the spacing between the lenses to correspond to the actual optical path length.) Single thin lens mode matching will first be examined.

Equations (B14) and (B15) give the location and focal length of the single thin lens that will match the modes. This lens has a 95.25-centimeter focal length, but it is located 1.23 centimeters to the left of the plane surface of the laser output mirror (i.e., within the laser cavity). Since this is physically impossible, two lenses must be used for mode matching.

If lenses with focal lengths of 12.70 and 19.05 centimeters (5 and 7.5 in.) are available, equations (B16) and (B17) show that mode matching is achieved with a 19.05-centimeter-focal-length thin lens placed 11.03 centimeters to the right of the laser output mirror and a 12.70-centimeter-focal-length thin lens placed 45.29 centimeters to the right of the laser output mirror. The intermediate waist radius w_{ox} is 51.29 micrometers. All waist radii with their positions and the positions of the thin lenses are shown in figure 17(b). These numerical values were obtained by rounding the actual values to two decimal places.

Finally, to adjust the lens spacing for finite lens thickness, increase the distance between the lenses by the increase in the optical path length (optical path length = actual path length x refractive index). This optical system has the required beam radius in the probe volume (62.5 μm), and the waists are at the beams crossing point.

As an illustration of the error that can occur if the system is not properly mode-matched, this system without the mode-matching lenses would have a waist radius in the probe volume of about 40 micrometers and about a 15 percent change in the fringe spacing over a 1 millimeter distance.

APPENDIX C

LDV SIGNAL PROCESSOR

The electronics system used to measure the Doppler frequency (range, 10 to 80 MHz) is based on a commercial computing counter. This instrument is able to measure time intervals with an accuracy of ±1 nanosecond. This permits the measurement of a time interval equal to eight periods of an 80-megahertz signal to be made with an accuracy of 1 percent. Additional circuitry is necessary to condition the Doppler signal and to insure that only valid Doppler signals are used. A logic diagram of this circuitry (built from ECL integrated circuits) is shown in figure 18(a). The circuitry did not add any significant error to the time interval measurement. The principle of operation of the circuitry is similar to that described in reference 17.

The signal from the photomultiplier tube is amplified and sent through a dividing network (combination low-pass - high-pass filter), which splits the signal into two parts. One output of the dividing network contains the part of the signal with frequency components less than 10-megahertz (the pedestal signal), and the other output contains the part of the signal with frequency components greater than 10 megahertz. If the amplitude of the pedestal signal of a Doppler burst exceeds a preset level, the circuitry causes that burst to be disregarded. This is to control the number of velocity measurements of large particles, which may not accurately follow the flow. The high-frequency signal is sent through a high-pass filter (5, 10, 20, or 40 MHz) to remove the remaining part of the pedestal and through a low-pass filter (50 or 80 MHz) to reduce the shot noise. It is then applied to a limiter circuit that produces a square wave output with transitions at the zero-crossing times of the input signal. This signal is also sent to Schmitt trigger 1, which has an adjustable threshold. (The logic diagram is shown in fig. 18(a), and selected waveforms are shown in figs. 18(b) and (c).) Whenever the amplitude of the Doppler signal exceeds the threshold of Schmitt trigger 1 (e.g., at time t_0), a short pulse is generated that resets flip-flop 1. The next transition (with positive slope) of the limiter output (e.g., at time t_1) causes the flip-flop to change states. The resulting low to high transition of the output of the flip-flop is used to clock a synchronous divide-by-eight counter. Succeeding cycles of the Doppler input signal with amplitudes that exceed the threshold of the Schmitt trigger result in a repetition of the process of resetting the flip-flop and clocking the divide-by-eight counter.

The initial state of the divide-by-eight counter is chosen so that its output changes from a low state to a high state on the 2nd pulse (at time t_2) and the 10th pulse (at time t_{10}) applied to its input. The computing counter measures the time interval $T = t_{10} - t_2$ (which is related to the Doppler frequency by $f_D = 8/T$).

Doppler signals are frequently encountered that have fewer than 10 consecutive cycles with amplitudes above the threshold of the Schmitt trigger. These may be caused by very small particles, by particles passing through the edges of the probe volume, or by noise. The following logic circuitry is used to eliminate these signals. The divide-by-eight counter is preset by every low to high transition of the output of the limiter if flip-flop 1 has not been reset; that is, every cycle of the input signal that does not exceed the Schmitt trigger threshold results in a preset of the divide-by-eight counter on the next positive-slope zero-crossing of the limiter output. Thus, ordinary noise in the input merely causes a continual presetting of the divide-by-eight counter.

If the input signal contains at least two consecutive cycles above the threshold of Schmitt trigger 1, the output of the divide-by-eight counter switches to the high state and is sent to one input of OR gate 2. The second input to this gate is taken from the output of the 1-microsecond, one-shot multivibrator (OSM) 1, which is in its low state at this time. The output of OR gate 2 is simultaneously applied to the clock (C) inputs of flip-flop 2, the 1-microsecond OSM 1 (through an AND gate), and the 800-nanosecond OSM. The 1-microsecond OSM 1 is not activated because the output of flip-flop 2 is low. (The gate delay time of flip-flop 2 prevents its output from switching to its high state until after the 1-microsecond OSM 1 is triggered.) The next low-to-high transition of the output of the divide-by-eight counter (shown in fig. 18(b) at time t_{10} with $t_{10} - t_2 = 200$ ns) passes through OR gate 2 and clocks 1-microsecond OSM 1. This second low-to-high transition has no effect on flip-flop 2 (whose output is already in its high state), or on the 800-nanosecond OSM.

The output of 1-microsecond OSM 1, as mentioned, is applied to one input of OR gate 2. The output of OR gate 2 is forced high for 1 microsecond starting at time t_{10}. This prevents any further output signal from the divide-by-eight counter from passing through OR gate 2 for 1 microsecond after time t_{10}.

The inverted output from OR gate 2 is delayed by 820 nanoseconds by a 206-meter coaxial cable (RG 63B). The output of the delay line is applied to one input of NOR gate 3. The other inputs of NOR gate 3 are used to control whether the signal from the delay line is allowed to go to the computing counter. The idea is to prevent input signals with less than 10 consecutive cycles above the Schmitt trigger threshold from reaching the computing counter. This is accomplished by considering as valid signals only those outputs from the divide-by-eight counter with two consecutive low-to-high transitions (i.e., at t_2 and t_{10}) before the divide-by-eight counter is preset. (Recall that the divide-by-eight counter is preset by any signal that is less than the threshold of the Schmitt trigger.)

If the two inputs to the output NOR gate (other than the input from the delay line) are low, the signal from the delay line will pass through the gate, and the time interval, $T = t_{10} - t_2$, will be measured by the computing counter. If either of these inputs is high, no signal will reach the computing counter. One of these control inputs is the output of a

three-input OR gate (OR gate 3). If any one of these inputs is high, NOR gate 3 will be inhibited. One of these inputs is from the negated output of 1-microsecond OSM 1. This input will be low for 1 microsecond after t_{10}. The second input to OR gate 3 is from the negated output of 1-microsecond OSM 2, which is triggered by the trailing edge of the pulse from the 800 nsec OSM. The output from the 1-microsecond OSM 1 and the negated output of the 800 nsec OSM are sent to NOR gate 2 whose output is applied to the D input of 2 microsecond OSM 1. (Note that this signal coincides with the time interval T that is to be measured by the computing counter.)

If a reset pulse is generated after the second input cycle at t_2 and before the 10th input cycle at t_{10}, the 2 microsecond OSM 1 is triggered. The resulting 2-microsecond pulse would not allow NOR gate 3 to open; this feature prevents input signals with less than 10 consecutive cycles above the Schmitt trigger threshold from reaching the computing counter. This 2-microsecond pulse is also fed back to an OR gate which holds the divide-by-eight counter in its preset state for the 2-microsecond period. With 10 or more cycles above the Schmitt trigger threshold, the output NOR gate is opened from time t_{10} + 800 nanosecond to time t_2 + 1 microsecond; this is a time interval equal to $t_{10} - t_2$ + 200 nanoseconds, which brackets the delayed output of the divide-by-eight counter. Thus, only valid time intervals are measured by the computing counter.

The pedestal component of the Doppler signal is split from the high-frequency part of the signal and is sent to a Schmitt trigger. If the pedestal amplitude is above the threshold of the Schmitt trigger, a 2-microsecond OSM is triggered, which closes the output NOR gate for this time, thus preventing signals with large pedestal amplitudes from reaching the computing counter.

REFERENCES

1. Yeh, H.; and Cummins, H. Z.: Localized Fluid Flow Measurements with an He-Ne Laser Spectrometer. Appl. Phys. Lett., vol. 4, no. 10, May 1964, pp. 176-178.

2. Thompson, H. D.; and Stevenson, W. H., eds.: Proceedings of the Second International Workshop on Laser Velocimetry. Vols. 1 and 2, H. D. Thompson and W. H. Stevenson eds., Bull. No. 144, Purdue Univ., 1974.

3. Wisler, D. C.; and Mossey, P. W.: Gas Velocity Measurements within a Compressor Rotor Passage Using the Laser Doppler Velocimeter. ASME Paper 72-WA/GT-2, Nov. 1972.

4. Goldman, Louis J.; Seasholtz, Richard G.; and McLallin, Kerry L.: Velocity Surveys in a Turbine Stator Annular-Cascade Facility Using Laser Doppler Techniques. NASA TM X-8269, 1976.

5. Seasholtz, Richard G.: Laser Doppler Velocimeter Measurements in a Turbine Stator Cascade Facility. Proceedings of the Second International Workshop on Laser Velocimetry. Vol. 2, H. D. Thompson and W. H. Stevenson, eds., Bull. No. 144, Purdue Univ., 1974, pp. 199-215.

6. McLaughlin, D. K.; and Tiederman, W. G.: Biasing Correction for Individual Realization of Laser Anemometer Measurements in Turbulent Flows. Phys. Fluids, vol. 16, no. 12, Dec. 1973, pp. 2082-2088.

7. Brayton, D. B.; and Goethert, W. H.: A New Dual-Scatter Laser Doppler-Shift Velocity Measuring Technique. ISA Trans., vol. 10, no. 1, 1971, pp. 40-50.

8. Hanson, S.: Broadening of the Measured Frequency Spectrum in a Differential Laser Anemometer Due to Interference Plane Gradients. J. Phys. D., vol. 6, no. 1, Jan. 1973, pp. 164-171.

9. Yariv, Amnon: Introduction to Optical Electronics. Holt, Rinehart, & Winston, Inc., 1971.

10. Kerker, Milton: The Scattering of Light and Other Electromagnetic Radiation. Academic Press, 1969.

11. Maxwell, Barry R.: Particle Flow in Turbomachinery with Application to Laser-Doppler Velocimetry. AIAA J., vol. 12, no. 10, Oct. 1974, pp. 1297-1298.

12. Maxwell, Barry R.: Tracer Particle Flow in a Compressor Rotor Passage with Application to LDV. AIAA J., vol. 13, no. 9, Sept. 1975, pp. 1141-1142.

13. Lanz, O.; Johnson, C. C.; and Morikawa, S.: Directional Laser Doppler Velocimeter. Appl. Optics, vol. 10, no. 4, April 1971, pp. 884-888.

14. Smith, Warren J.: Modern Optical Engineering. McGraw-Hill Book Co., Inc., 1966.

15. Sinclair, Douglas C.; and Bell, W. Earl: Gas Laser Technology. Holt, Rinehart, & Winston, Inc., 1969.

16. Francois, G. E.; Librecht, F. M.; and Engelen, J. J.: Mode Matching with a Single Thin Lens. Appl. Optics, vol. 10, no. 5, May, 1971, pp. 1157-1159.

17. Iten, P. D.; and Mastner, J.: A Laser Doppler Velocimeter Offering High Spatial and Temporal Resolution. Flow: Its Measurement and Control in Science and Industry. Vol. 1, Pt. 2, Instrum. Soc. Am., 1974, pp. 1007-1013.

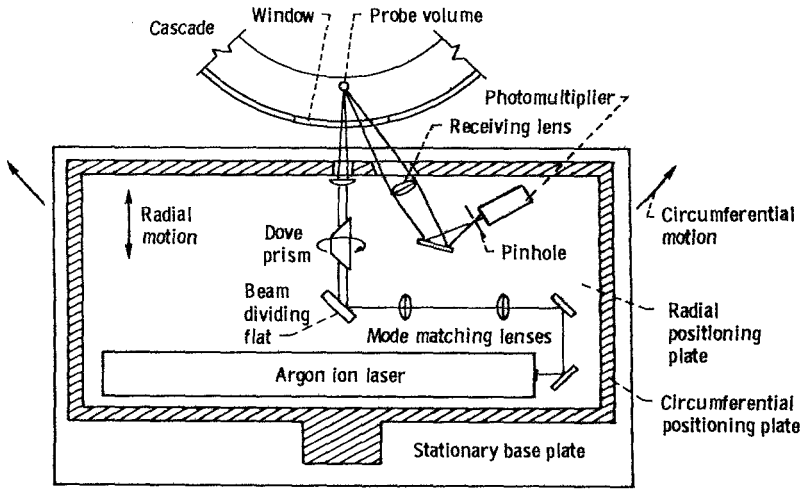

Figure 1. - Top view of laser Doppler velocimeter optics used for mapping flow in annular turbine stator cascade.

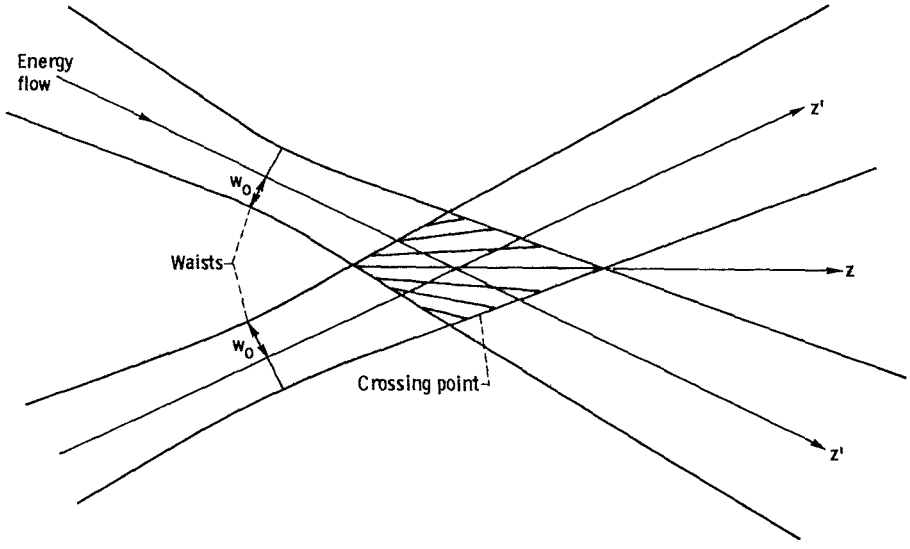

Figure 2. - Probe volume fringe pattern with beam waists before crossing point showing gradient in fringe spacing.

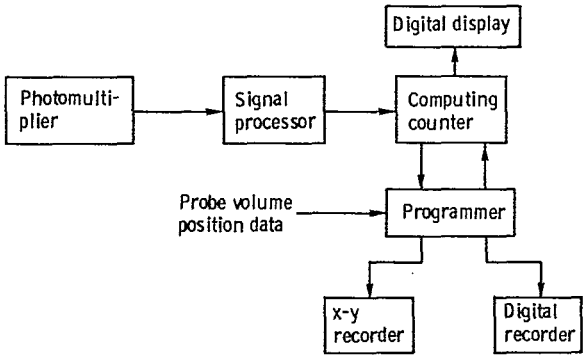

Figure 3. - Block diagram of signal processing and data reduction system.

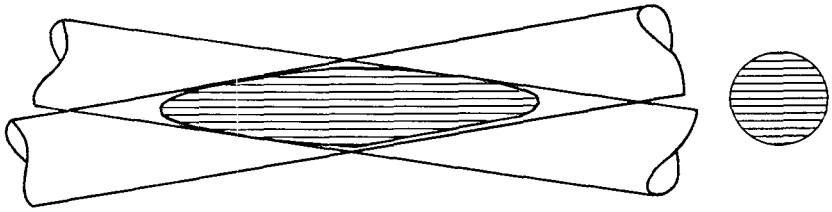

(a) True ellipsoidal probe volume.

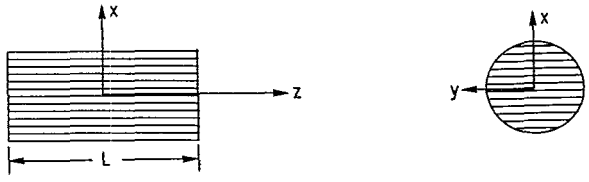

(b) Cylindrical probe volume (approximation to ellipsoidal probe volume).

Figure 4. - Probe volume showing fringes generated by crossed laser beams.

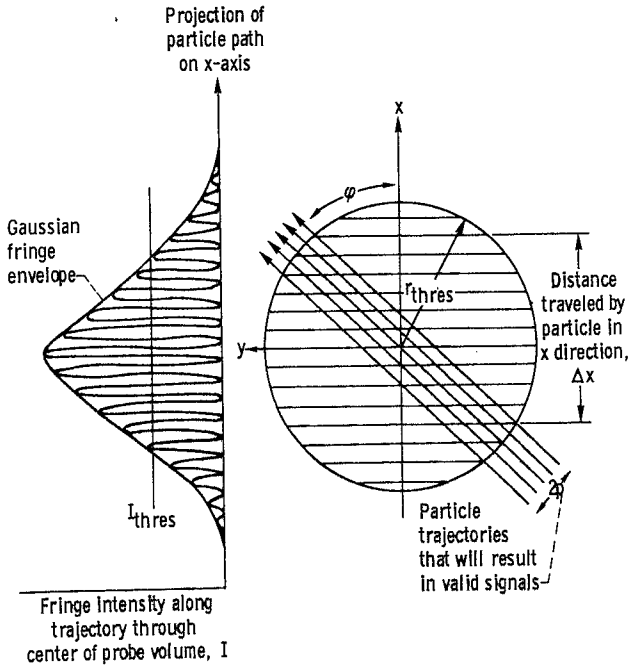

Figure 5. - Fringe intensity profile along trajectory through center of probe volume.

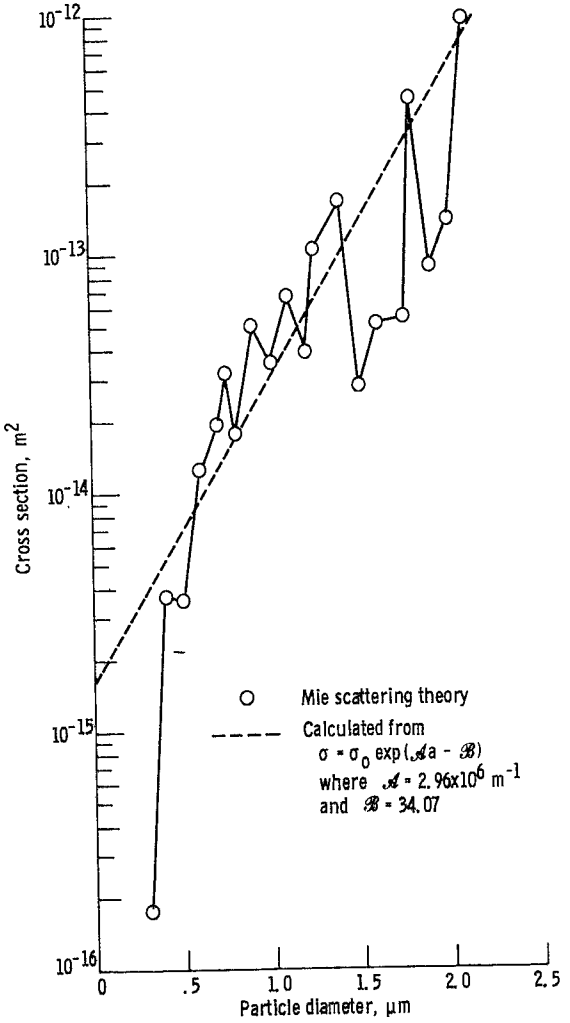

Figure 6. - Backscatter cross section for spherical particle. Refractive index, 1.4; wavelength, 0.5145 nanometer.

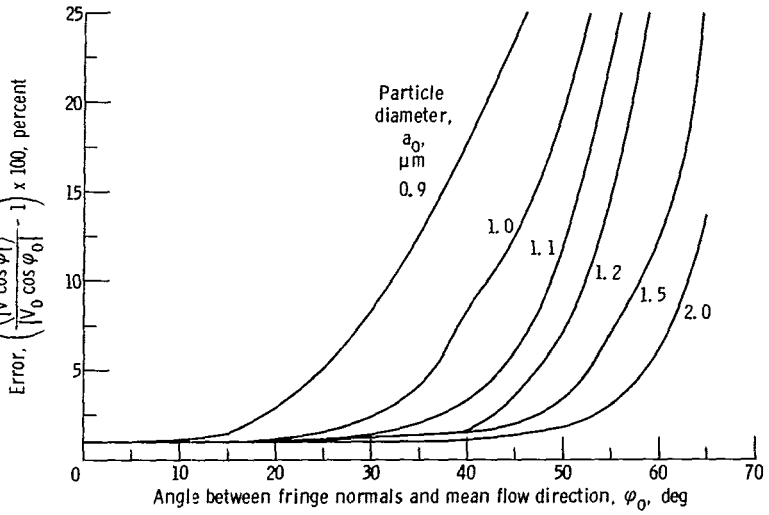

Figure 7. - Error in mean value of velocity component as function of angle between fringe normals and mean flow direction with particle diameter as parameter. Ratio of trigger threshold power to incident power, 1×10^{-7}; standard deviation of particle size distribution, 0; probe volume diameter, 125 micrometers; fringe spacing, 6.25 micrometers; turbulence intensity, 0.1.

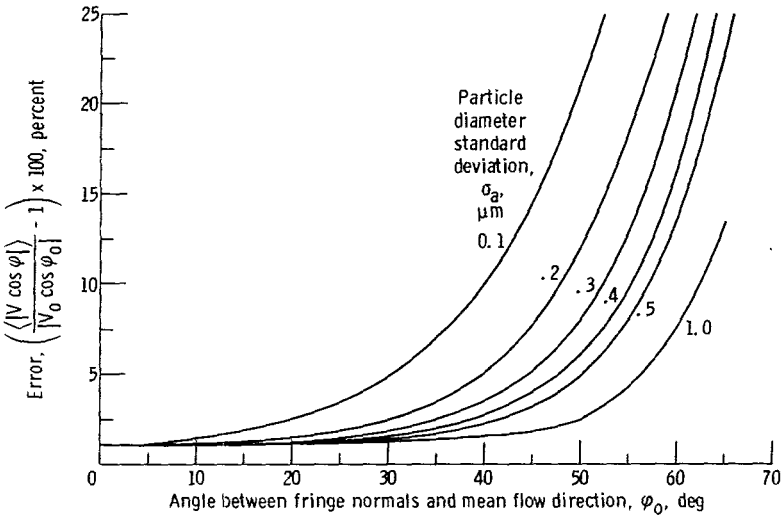

Figure 8. - Error in mean value of velocity component as function of angle between fringe normals and mean flow direction with particle diameter standard deviation as parameter. Ratio of trigger threshold power to incident power, 1×10^{-7}; mean particle diameter, 0.6 micrometer; probe volume diameter, 125 micrometers; fringe spacing, 6.25 micrometers; turbulence intensity, 0.1.

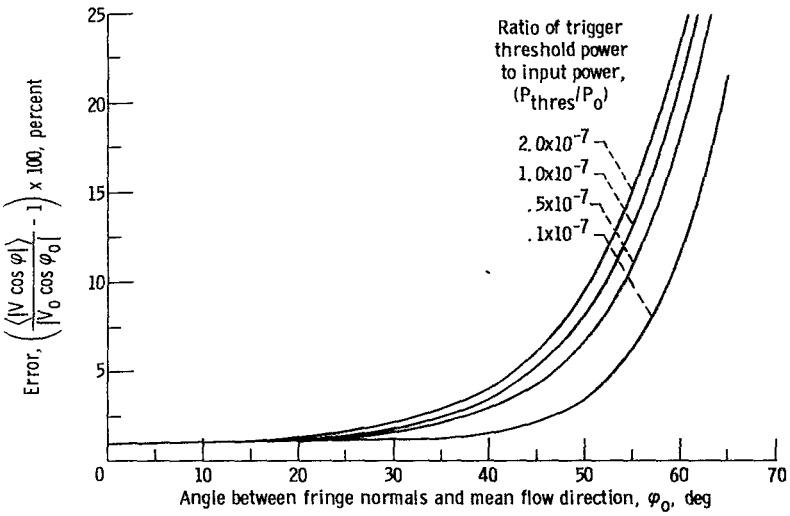

Figure 9. - Error in mean value of velocity component as function of angle between fringe normals and mean flow direction with ratio of trigger threshold power to input power as parameter. Mean particle diameter, 0.6 micrometer; standard deviation of particle size distribution, 0.3 micrometer; probe volume diameter, 125 micrometers; fringe spacing, 6.25 micrometers; turbulence intensity, 0.1.

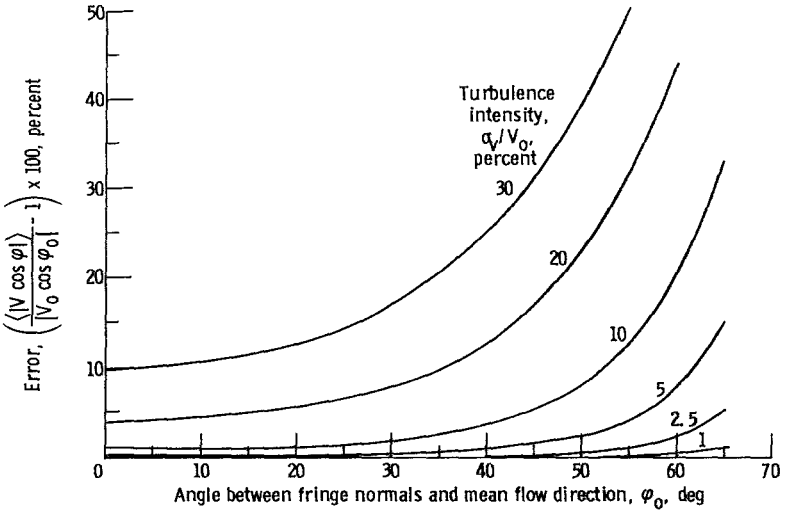

Figure 10. - Error in mean value of velocity component as function of angle between fringe normals and mean flow direction with turbulence intensity as parameter. Ratio of trigger threshold power to incident power, 1×10^{-7}; particle mean diameter, 0.6 micrometer; standard deviation of particle size distribution, 0.3 micrometer; probe volume diameter, 125 micrometers; fringe spacing, 6.25 micrometers.

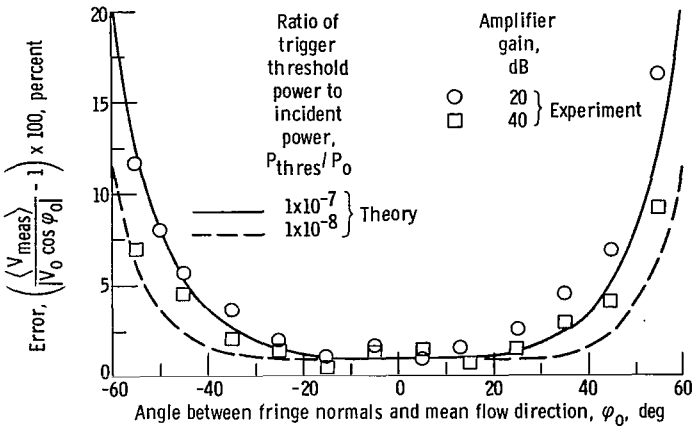

Figure 11. - Comparison of theoretical and measured error in turbulent jet of mean value of velocity component as function of angle between fringe normals and mean flow direction. Turbulence intensity, 0.1; particle mean diameter, 0.6 micrometer; standard deviation of particle size distribution, 0.3 micrometer; probe volume diameter, 125 micrometers; fringe spacing, 6.25 micrometers.

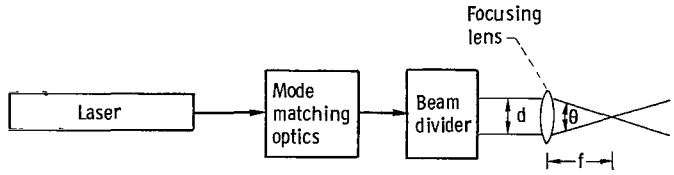

Figure 12. - General dual scatter transmitting optical system.

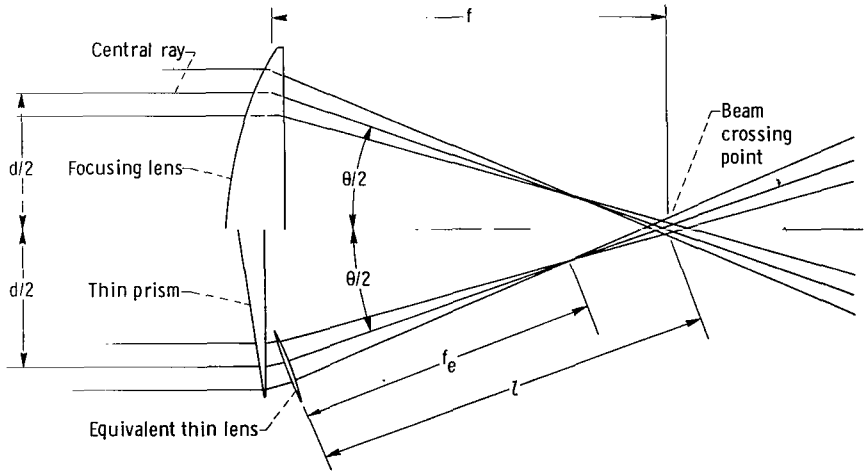

Figure 13. - Focusing lens with equivalent thin prism plus thin lens.

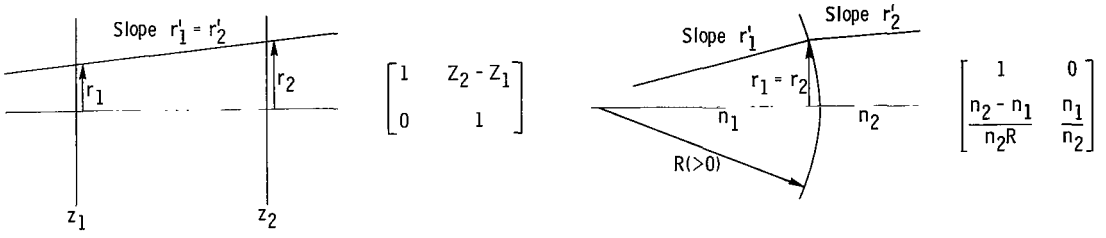

(a) Homogeneous medium from z_1 to z_2.

(b) Spherical interface between media with refractive indices n_1 and n_2.

Figure 14. - Ray paths and corresponding ABCD matrices.

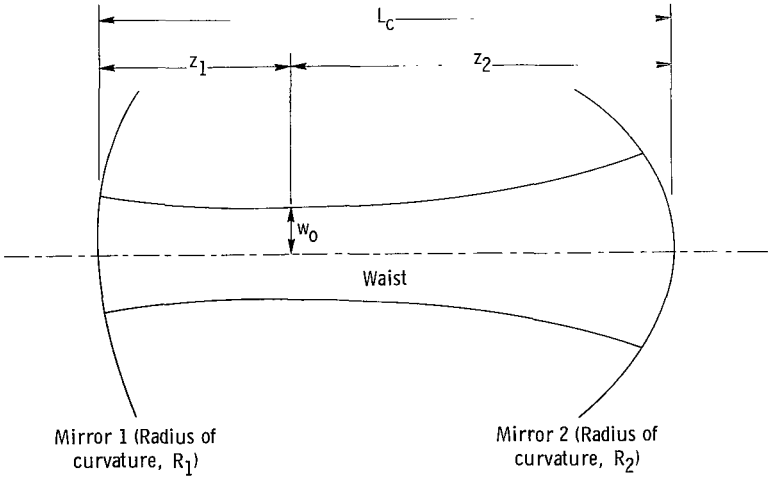

Figure 15. - Laser cavity with mirror radii R_1 and R_2 (both >0 as drawn).

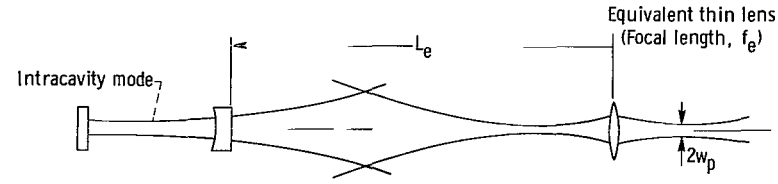

(a) Optical system to be mode matched.

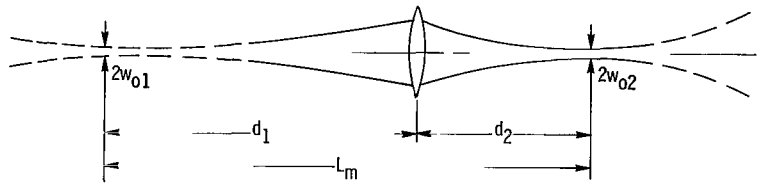

(b) Mode match with single, thin lens of focal length f_m.

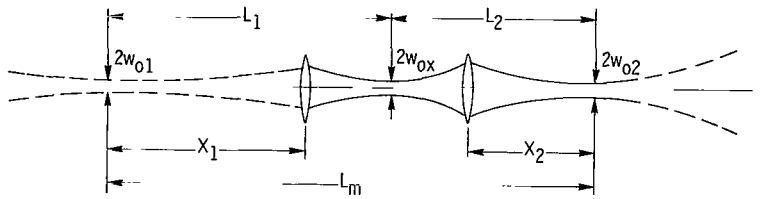

(c) Mode match with two thin lenses.

Figure 16. - Mode matching LDV optical system.

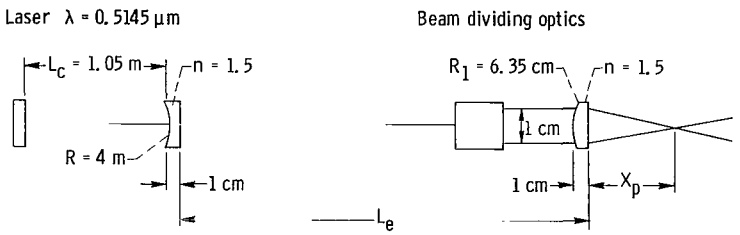

(a) LDV system to be mode matched.

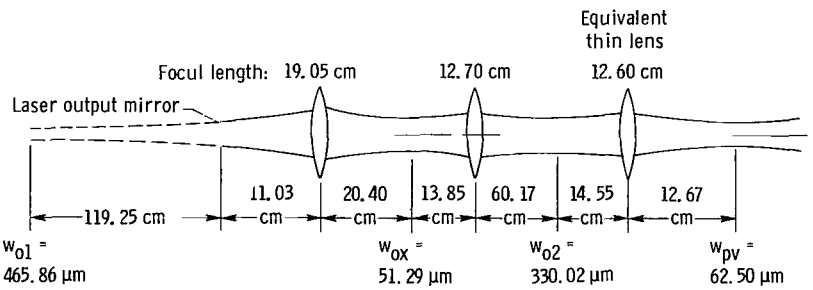

(b) Solution of mode matching problem showing positions of thin lenses and positions and radii of waists.

Figure 17. - Example of mode matching a specific laser Doppler velocimeter optical system.

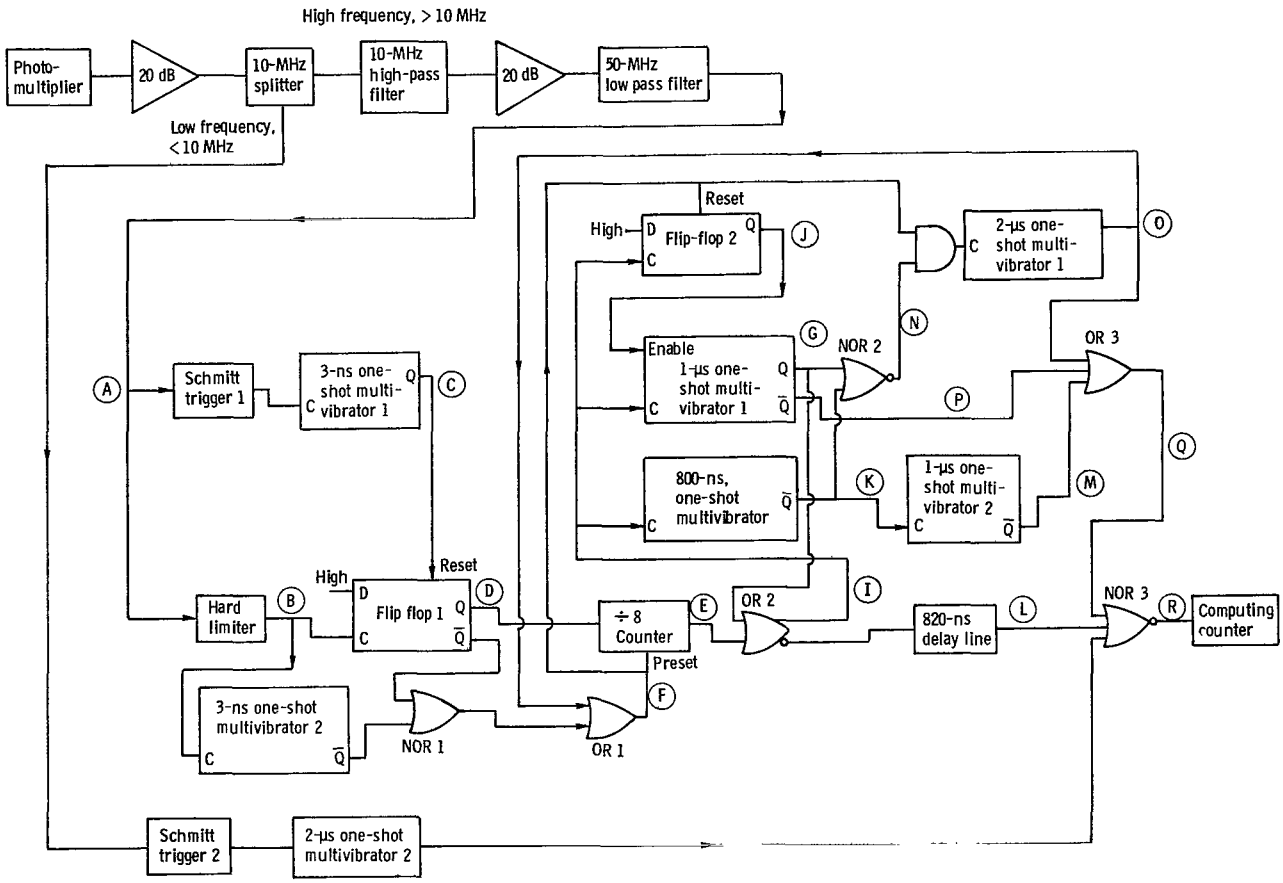

(a) Logic diagram.

Figure 18. - Laser Doppler velocimeter signal processor.

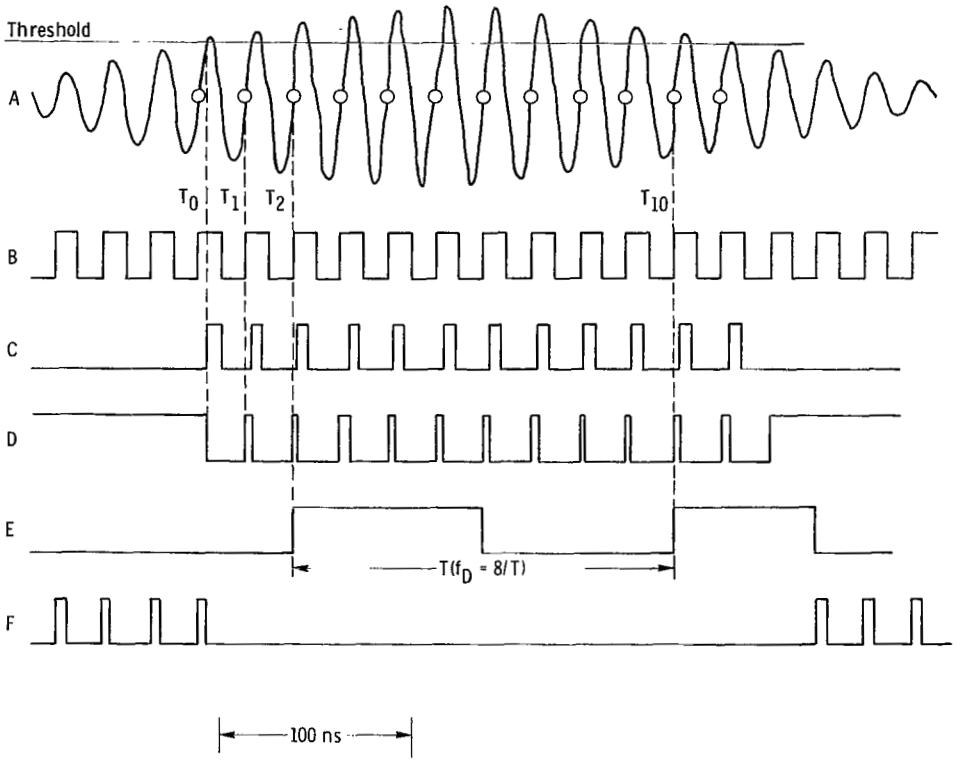

(b) Signal waveforms (letters refer to labeled points in part (a)).

Figure 18. - Continued.

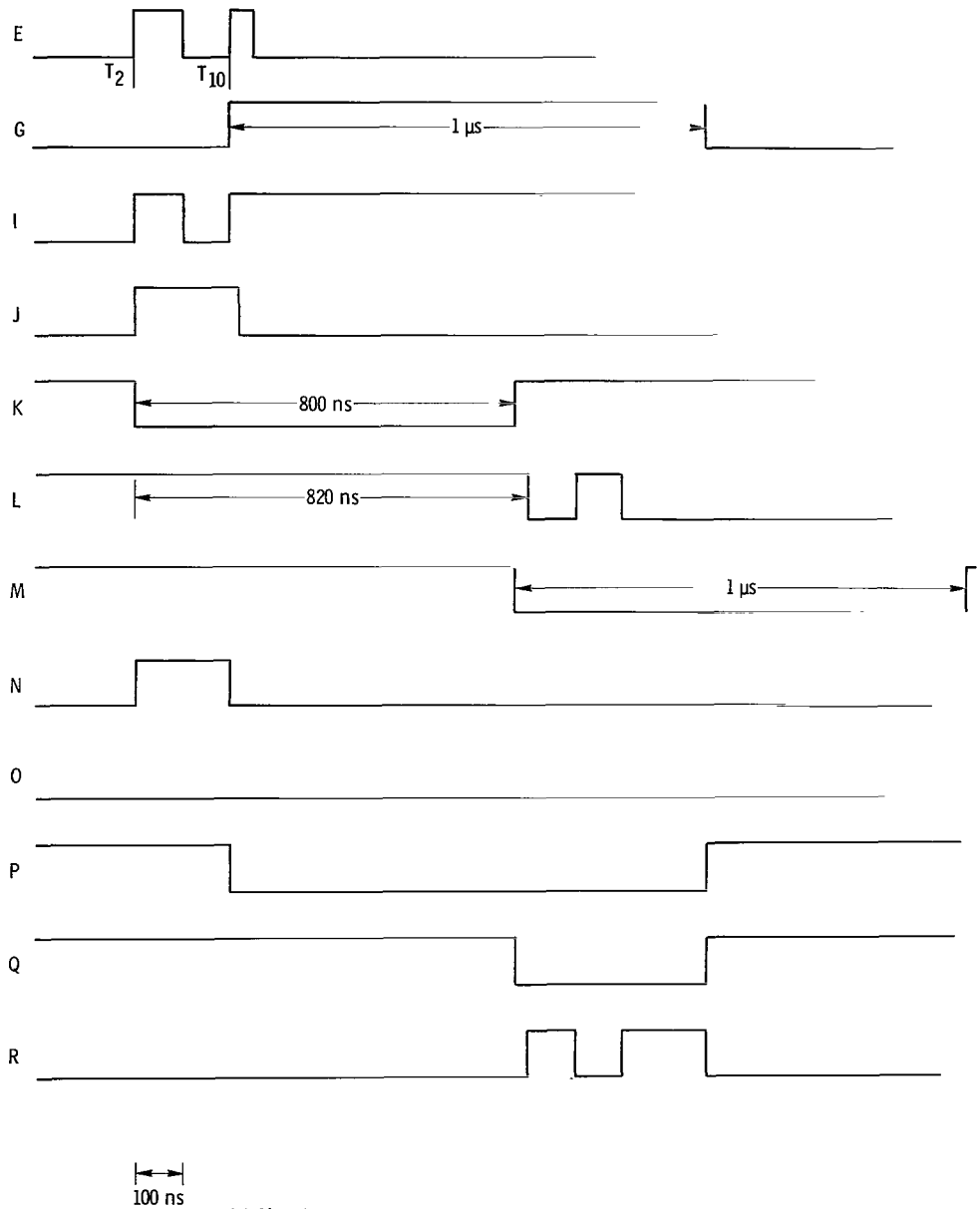

(c) Signal waveforms (letters refer to labeled points in part (a)).

Figure 18. - Concluded.

"The aeronautical and space activities of the United States shall be conducted so as to contribute . . . to the expansion of human knowledge of phenomena in the atmosphere and space. The Administration shall provide for the widest practicable and appropriate dissemination of information concerning its activities and the results thereof."

—NATIONAL AERONAUTICS AND SPACE ACT OF 1958

NASA SCIENTIFIC AND TECHNICAL PUBLICATIONS

TECHNICAL REPORTS: Scientific and technical information considered important, complete, and a lasting contribution to existing knowledge.

TECHNICAL NOTES: Information less broad in scope but nevertheless of importance as a contribution to existing knowledge.

TECHNICAL MEMORANDUMS: Information receiving limited distribution because of preliminary data, security classification, or other reasons. Also includes conference proceedings with either limited or unlimited distribution.

CONTRACTOR REPORTS: Scientific and technical information generated under a NASA contract or grant and considered an important contribution to existing knowledge.

TECHNICAL TRANSLATIONS: Information published in a foreign language considered to merit NASA distribution in English.

SPECIAL PUBLICATIONS: Information derived from or of value to NASA activities. Publications include final reports of major projects, monographs, data compilations, handbooks, sourcebooks, and special bibliographies.

TECHNOLOGY UTILIZATION PUBLICATIONS: Information on technology used by NASA that may be of particular interest in commercial and other non-aerospace applications. Publications include Tech Briefs, Technology Utilization Reports and Technology Surveys.

Details on the availability of these publications may be obtained from:

SCIENTIFIC AND TECHNICAL INFORMATION OFFICE

NATIONAL AERONAUTICS AND SPACE ADMINISTRATION

Washington, D.C. 20546